BIOCHEMISTRY
including biophysical chemistry & molecular biology

Article

pubs.acs.org/biochemistry

Inverse Thio Effects in the Hepatitis Delta Virus Ribozyme Reveal that the Reaction Pathway Is Controlled by Metal Ion Charge Density

Pallavi Thaplyal,[†,§] Abir Ganguly,[‡,⊥] Sharon Hammes-Schiffer,[*,‡] and Philip C. Bevilacqua[*,†]

[†]Department of Chemistry and Center for RNA Molecular Biology, The Pennsylvania State University, University Park, Pennsylvania 16802, United States

[‡]Department of Chemistry, University of Illinois at Urbana−Champaign, Urbana, Illinois 61801, United States

Supporting Information

ABSTRACT: The hepatitis delta virus (HDV) ribozyme self-cleaves in the presence of a wide range of monovalent and divalent ions. Prior theoretical studies provided evidence that self-cleavage proceeds via a concerted or stepwise pathway, with the outcome dictated by the valency of the metal ion. In the present study, we measure stereospecific thio effects at the nonbridging oxygens of the scissile phosphate under a wide range of experimental conditions, including varying concentrations of diverse monovalent and divalent ions, and combine these with quantum mechanical/molecular mechanical (QM/MM) free energy simulations on the stereospecific thio substrates. The R_P substrate gives large normal thio effects in the presence of all monovalent ions. The S_P substrate also gives normal or no thio effects, but only for smaller monovalent and divalent cations, such as Li^+, Mg^{2+}, Ca^{2+}, and Sr^{2+}; in contrast, sizable inverse thio effects are found for larger monovalent and divalent cations, including Na^+, K^+, NH_4^+, and Ba^{2+}. Proton inventories are found to be unity in the presence of the larger monovalent and divalent ions, but two in the presence of Mg^{2+}. Additionally, rate−pH profiles are inverted for the low charge density ions, and only imidazole plus ammonium ions rescue an inactive C75Δ variant in the absence of Mg^{2+}. Results from the thio effect experiments, rate−pH profiles, proton inventories, and ammonium/imidazole rescue experiments, combined with QM/MM free energy simulations, support a change in the mechanism of HDV ribozyme self-cleavage from concerted and metal ion-stabilized to stepwise and proton transfer-stabilized as the charge density of the metal ion decreases.

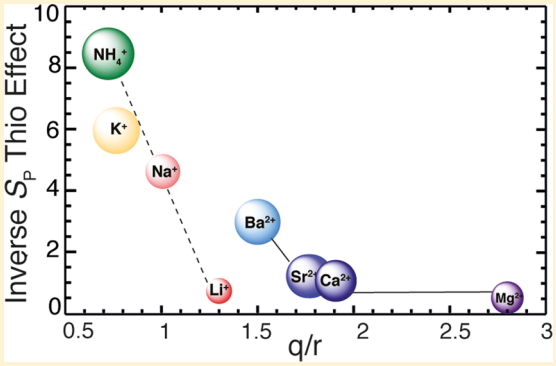

Catalytic RNAs can be divided into larger ribozymes that use exogenous substrates and leave reaction termini with a 5′-phosphate and 3′-OH, and smaller ribozymes that self-cleave and leave termini with a 5′-OH and 2′,3′-cyclic phosphate.[1,2] The roles of metal ions in RNA catalysis are complex and include both folding and catalytic contributions.[3] The larger ribozymes almost always show high specificity for Mg^{2+}, with much revealed about their mechanisms from crystal structures and thio effect and metal ion rescue studies.[4] For the smaller ribozymes, the roles of metal ions are both less specific and less well understood.[1−3]

The self-cleaving ribozymes do not exhibit strong specificity for a particular ion type or even ion valency. For instance, a wide variety of divalent ions can fold small ribozymes into an active form and in some cases act as a general base. Additionally, most small ribozymes are active in the presence of high concentrations of monovalent ions alone. The hairpin,[5] hepatitis delta virus (HDV),[6,7] hammerhead,[5] varkud satellite (VS),[5] glucosamine-6-phosphate activated (glmS),[8] and twister[9] ribozymes, for instance, are active in molar amounts of monovalent ions. Furthermore, hairpin,[10,11] glmS,[8] and twister[9] ribozymes are fully active in the presence of micromolar to millimolar amounts of $[Co(NH_3)_6]^{3+}$,[10,11] which is exchange inert and thus cannot form inner-sphere interactions.[12] In contrast, in the HDV and hammerhead ribozymes, $[Co(NH_3)_6]^{3+}$ is a competitive inhibitor of Mg^{2+} but tolerated in the presence of catalytic amounts of Na^+.[6,13−15] In some cases, contributions of divalent ions to folding and catalysis have been quantified. For the HDV ribozyme, the rate of reaction is ∼3000-fold slower in 1 M NaCl than in saturating Mg^{2+}.[6,7] In particular, we parsed this cleavage mechanism into a multichannel mechanism and found that divalent ions contribute ∼125-fold over monovalent ions toward folding, and ∼25-fold toward chemistry.[16] Similar contributions of divalent ions toward chemistry have been reported for the hammerhead ribozyme.[17,18] We recently used thio effect and metal ion rescue experiments with Cd^{2+} to test for interaction between the pro-R_P oxygen and catalytic divalent metal ion as modeled into a precleaved HDV ribozyme crystal structure.[19] Observation of unique metal ion contributions in disparate ribozymes indicates that metal ions may make unique contributions to catalysis and even affect which reaction pathway is used by the ribozyme.

Received: February 24, 2015
Published: March 23, 2015

DOI: 10.1021/acs.biochem.5b00190
Biochemistry 2015, 54, 2160−2175

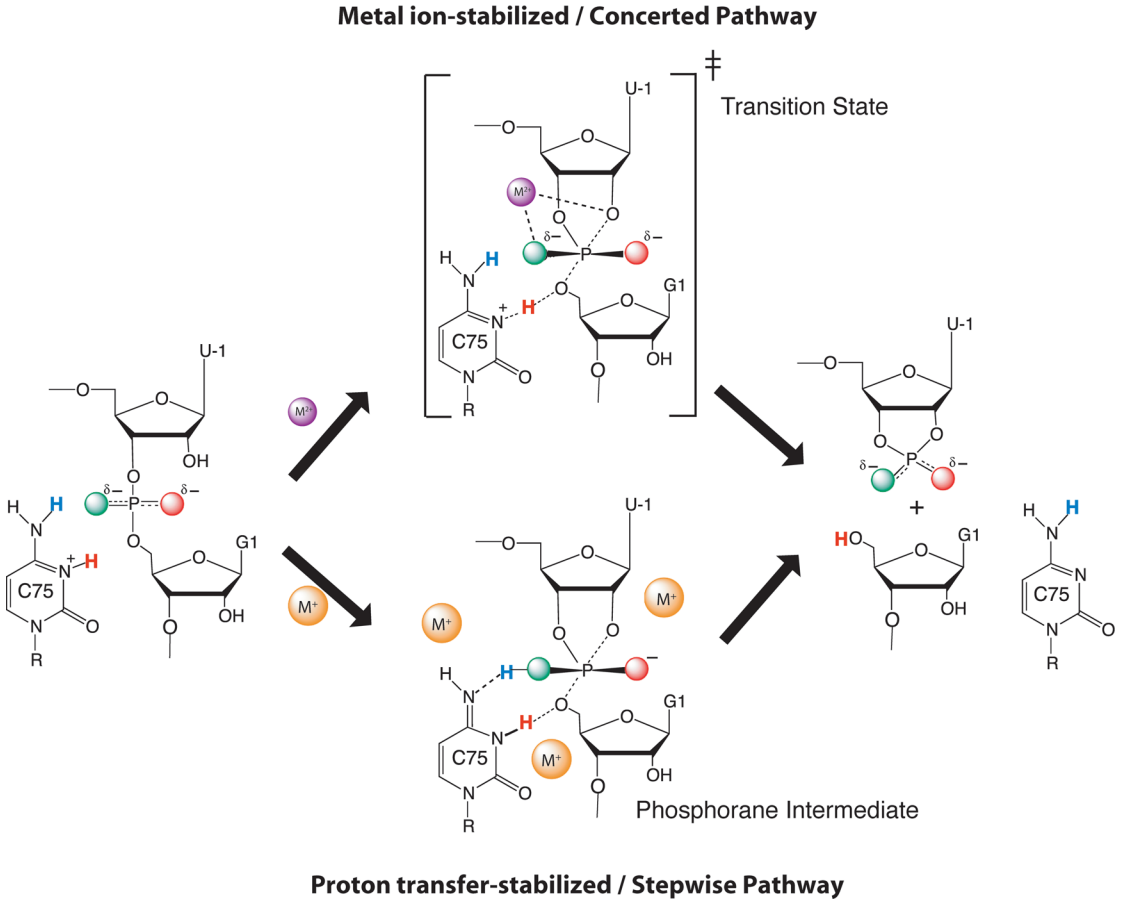

Figure 1. Distinct reaction pathways in the presence of divalent and monovalent ions. The *pro*-R_P and *pro*-S_P oxygen atoms are shown in green and red, respectively. The catalytic high charge density divalent ion is placed at its crystallographic position near the *pro*-R_P oxygen and the 2′-OH[37] as supported by metal ion rescue,[19] while various low charge density ions (here monovalent ions) are shown at several sites to represent their diffuse nature when present in the region of the active site. The N3 and N4 hydrogen atoms on C75 are shown in red and cyan, respectively. Ground state interactions of the Mg^{2+} ion are shown in Figure 4 but are not depicted here in the common reactant state.

The HDV ribozyme is a small self-cleaving RNA that is widespread, occurring in human viruses, in the human genome, and in many different organisms.[20−22] The mechanism of the HDV ribozyme involves in-line attack by the 2′-OH of U-1, which is activated by a Mg^{2+} ion acting as a general base, and protonation of the leaving group by $C75^+$ acting as a general acid.[23] This mechanism has received extensive support from both experiments[6,24] and calculations.[25−27] Active participation of nucleobases in general acid−base chemistry of diverse ribozymes is ubiquitous as supported by experiments, notably from Raman crystallography,[28−30] as well as calculations.[31,32]

Further evidence for distinct reaction pathways of the HDV ribozyme in the presence of different metal ions has been provided by rate−pH profiles and proton inventory studies.[6,33,34] The rate−pH profile in the presence of Na^+ alone is inverted (i.e., related by a reflection about a vertical axis) relative to that in the presence of Mg^{2+} or Ca^{2+}.[6,35] In particular, in the presence of Mg^{2+} the logarithm of the observed rate constant is found to increase linearly as a function of pH until pH ∼ 7.0 and then plateau at a higher pH, while in the presence of Na^+ the observed rate constant shows no dependence on pH between pH 4.5−5.5 and then decreases log−linearly above pH 5.5. In addition, in the presence of Na^+ the reaction has a proton inventory of 1 supporting a stepwise reaction, whereas in the presence of Mg^{2+} the reaction has a proton inventory of 2 supporting a concerted reaction.[33,34] Recent quantum mechanical/molecular mechanical (QM/MM) free energy simulations from our research groups further support unique pathways in the presence of Mg^{2+} and Na^+ and provide chemical details for each pathway,[36] which can be tested by additional experiments. In particular, calculations with a Mg^{2+} ion at the active site support a concerted reaction that goes through a metal ion-stabilized dianionic transition state, while calculations in the presence of Na^+ indicate a stepwise reaction with a proton transfer-stabilized phosphorane intermediate (Figure 1).[36] Moreover, in the simulations of the stepwise mechanism, two distinct proton transfers are performed by $C75^+$: to and from the *pro*-R_P nonbridging oxygen to form and break down the phosphorane intermediate and to the 5′-bridging oxygen to stabilize the product.

Early investigations of thio effects in monovalent ions were performed by Perrotta and Been for both the genomic and antigenomic HDV ribozymes using a mixture of R_P and S_P substrates,[7] where "R_P/S_P substrate" refers to RNA containing a sulfur substitution at the nonbridging *pro*-R_P/S_P oxygen on the scissile phosphate. More recently, we reported thio effects for the genomic HDV ribozyme in a limited set of monovalent ions but with stereopure R_P and S_P substrates.[19] Perrotta and Been reported an inverse thio effect of ∼3-fold for the thio substrate mixture in 4 M NaCl,[7] and our studies revealed that this inverse thio effect is specific to the S_P substrate.[19] In addition, for the thio substrate mixture and the genomic HDV ribozyme in the

DOI: 10.1021/acs.biochem.5b00190
Biochemistry 2015, 54, 2160−2175

presence of NH_4^+ ion, they reported an inverse thio effect of ~18-fold, much larger in magnitude than for any of the other monovalent ions tested.[7]

Herein, we provide a systematic study of stereospecific thio effects at the scissile phosphate of the genomic HDV ribozyme in multiple concentrations of each of the monovalent ions Li^+, Na^+, K^+, and NH_4^+, as well as in 10 mM of the divalent ions Ca^{2+}, Sr^{2+}, and Ba^{2+}, and compare our results to prior thio effects in the presence of 10 mM Mg^{2+}. We also conduct proton inventories in the presence of Li^+, NH_4^+, and Ba^{2+}, and compare to prior inventories in the presence of Na^+ and Mg^{2+}. In addition, we perform QM/MM free energy simulations of self-cleavage for the R_P and S_P substrates with Mg^{2+} or Na^+ bound at the catalytic site and compare the results to our previous simulations for the oxo substrate. The combined experimental and theoretical observations support a change in the reaction pathway from concerted to stepwise as the charge density of the metal ion decreases.

MATERIALS AND METHODS

RNA Oligonucleotides and Ribozyme Construct. Our experiments utilize the same two-piece HDV ribozyme construct from our prior functional and structural studies that is fast reacting and has a reduced propensity to misfold.[19,37] A schematic of the secondary structure studied is provided as Figure S1, Supporting Information. The HDV ribozyme was prepared in two pieces as described earlier.[37] The first piece, designated the enzyme strand, is 64 nucleotides and spans the P2, P3, P1.1, P4, and the 3′-strand of P1. The enzyme strand was transcribed using T7 RNA polymerase from a hemiduplex template consisting of the top strand with the sequence 5′ TAA TAC GAC TCA CTA TA, and the bottom strand containing the sequence 5′GGT CCG CAT TCG CCA TTA CCT TTC GGA ATG TTG CCC AGC TTG CGC CGC GAG GAG GCT GCG GAC CTA TAG TGA GTC GTA TTA. The transcribed RNA was purified on an 8% polyacrylamide/7 M urea gel, visualized by brief UV shadowing, and excised from the gel. The RNA was eluted overnight at 4 °C into a 1 mL solution of 10 mM Tris-HCl (pH 7.5), 0.1 mM EDTA, and 250 mM NaCl (TEN_{250}), precipitated with 3 vol of ethanol, resuspended in double-distilled water, and stored at −20 °C.

The second piece, designated the substrate strand, is 11 nucleotides in length and comprises the 5′-strand of P1 and the cleavage site. The substrate strand was prepared by solid-phase synthesis (Integrated DNA Technologies) with the sequence 5′-UAU*GGC UUG CA, where the "*" indicates the site of cleavage and phosphorothioate substitution. The oligonucleotide was obtained as a mixture of diastereomers and separated into pure R_P and S_P diastereomers using reverse phase HPLC, as described.[19] Purified diastereomers were dried, resuspended in double distilled water, and stored at −20 °C. Samples were characterized before and during storage as described.[19]

The oxo and stereopure thio substrates were 5′-end radiolabeled for kinetic assays by treating with T4 polynucleotide kinase (New England Biolabs) and γ-^{32}P ATP. The labeled 11-mer substrates were purified on a 16% polyacrylamide/7 M urea gel. The RNA was excised from the gel, eluted overnight at 4 °C into a 1 mL solution of TEN_{250}, precipitated with 3 volumes of ethanol, resuspended in double distilled water, and stored at −20 °C.

Buffer Preparation. The following stock solutions were prepared: $M_{2X}E_{2X}/H_{2X}E_{2X}$ (50 mM MES or HEPES/0.2 M Na_2EDTA) and $MEM_{1.2X}/HEM_{1.2X}$ (25 mM MES or HEPES/0.1 M Na_2EDTA/1.2× MCl). The buffer for pH 5.0−6.5 was MES and for pH 6.5−8.5 was HEPES. The final metal chloride solutions' concentrations (1×) were variable and ranged from 250 mM to 4 M. A detailed description of the preparation of the buffers is described in our earlier studies.[34,38] The buffers were brought to the appropriate pH with HCl for low pH buffers or the hydroxide of the cation under study (i.e., NaOH, KOH, LiOH, or NH_4OH) for high pH buffers. The same buffers were also prepared in D_2O for the proton inventory experiments, details of which are described below.

Kinetic Assays. Reactions in the presence of monovalent ions were performed under conditions similar to those described for a one-piece ribozyme construct.[34] All monovalent ion-containing reactions contained 100 mM EDTA to chelate any polyvalent ion contaminants; EDTA binds Mg^{2+} relatively weakly, especially in high ionic strength and low pH, so large concentrations of EDTA are needed.[6,7,34] Prior to each experiment, 1 μL of substrate (~1 nM) and 4 μL of enzyme (~2 μM) were renatured at 55 °C for 10 min and cooled at room temperature for 10 min.[a] Subsequently, 4 μL of $M_{2X}E_{2X}$ of appropriate pH was added, followed by incubation of the reaction mixture at 37 °C for 2 min. The reaction was initiated by addition of 42 μL of prewarmed $MEM_{1.2X}/HEM_{1.2X}$ buffer. The total reaction volume was ~50 μL. The final reaction mixture contains 25 mM MES/HEPES, 100 mM Na_2EDTA, and 1× MCl. For the reaction in the presence of NaCl, the final sodium ion concentration is (1× + 0.2 M) Na^+, where the 0.1 M Na_2EDTA (final concentration) contributed the extra 0.2 M Na^+. At regular intervals, 3 μL time points were taken and quenched with 27 uL of formamide loading buffer (in 100 mM Tris-HCl (pH 8.0) to quench the reaction and help mobility of the bands on the gel), and immediately placed on powdered dry ice. A 9:1 ratio of loading buffer to sample, as opposed to the more typical 1:1 ratio, was used to dilute the high salt for the polyacrylamide gels.

For the reaction in the presence of divalent ions, a similar procedure was followed.[19] First, 1 μL of substrate (~1 nM) and 10 μL of enzyme (~2 μM) were renatured at 90 °C for 2 min and then cooled at room temperature for 10 min. Next, 5 μL of 500 mM NaMES/NaHEPES (50 mM final) buffer and 25 μL of double-distilled water were added, followed by incubation of the reaction mixture at 37 °C. A zero time point (1 μL) was removed and the reaction was initiated by addition of 10 μL of prewarmed divalent metal ion solution (10 mM final divalent ion). At regular intervals, 3 μL time points were taken and quenched with 3 μL formamide loading buffer (in 100 mM Tris-HCl (pH 8.0) and 20 mM Na_2EDTA) and immediately placed on powdered dry ice. Time points were fractionated on a 20% polyacrylamide/7 M urea. Gels were dried and visualized using a PhosphorImager (Molecular Dynamics). In the presence of divalent ions, the reactions were performed only for the oxo and the S_P substrates; thio effect studies on the R_P substrate would not help distinguish between the major models for the inverse thio effect (see Discussion).

Plots of fraction cleaved as a function of time were constructed and fit to the single-exponential equation:

$$f_{\text{cleaved}} = A + Be^{-k_{\text{obs}}t} \quad (1)$$

where f_{cleaved} is the fraction of substrate cleaved; $-B$ is the amplitude of the reaction (note that B itself is negative, so the amplitude is positive); $A + B$ is the burst phase ($A + B \approx 0$ for the reactions described herein); and k_{obs} is the observed first-

DOI: 10.1021/acs.biochem.5b00190
Biochemistry 2015, 54, 2160−2175

order rate constant for the reaction. For slow reactions (oxo substrate in the presence of Na^+, K^+, and NH_4^+; R_P substrate in the presence of Li^+, Na^+, and NH_4^+; and S_P substrate in the presence of 0.5 and 1 M Na^+ and NH_4^+ and all concentrations of K^+), the fraction cleaved versus time profiles were fit to a linear form of eq 1:

$$f_{\text{cleaved}} = (A + B) - Bk_{\text{obs}}t \quad (2)$$

where the fraction cleaved versus time profiles describe the initial linear phase of the reaction. The intercept of the line is "$A + B$" and corresponds to the burst phase ($A + B \approx 0$ in all cases herein, signifying the lack of a burst phase), while the slope of the line corresponds to $-Bk_{\text{obs}}$. To obtain k_{obs}, the slope of the line was divided by $-B$. The value of B was considered as -1 in all the cases described herein; in other words, the k_{obs} was set equal to the slope.[b] All kinetic parameters were obtained by nonlinear least-squares fitting of the reaction profiles using KaleidaGraph (Synergy Software).

Rate−pH profiles were plotted for reactions in the presence of Li^+, NH_4^+, and Ba^{2+} and fit to the logarithm of eq 3 to obtain the pK_a:

$$k_{\text{obs}} = \frac{k_{\text{max}}}{1 + 10^{\text{pH}-\text{p}K_a}} \quad (3)$$

where k_{obs} is the observed rate constant at a particular pH, and k_{max} is the maximal observed rate constant.

In all cases, control reactions with the enzyme omitted were conducted to account for background cleavage. The oxo and S_P substrates did not exhibit significant levels of background (<5% over 48 h) as compared to the amplitude of the reaction (between 25 and 90%); the R_P substrate showed some background at longer time points (∼5% in the presence of 4 M NH_4Cl) compared to the amplitude of the reaction (∼15%), which was corrected by subtraction.

Proton Inventories. Proton inventory experiments were performed in the presence of Li^+, Ba^{2+}, or NH_4^+ at pL= 5.4, as described previously.[33,34,38] All the buffers, metal ion mixtures, and RNA were prepared in either 100% H_2O or 100% D_2O. The pD was calculated according to eq 4:[39]

$$\text{pD} = \text{pH}_{\text{meter reading}} + 0.4 \quad (4)$$

The protocol for the proton inventory experiments was similar to that described above. The proton inventory experiments were performed in the plateau region of the rate-pH profile for Li^+, Ba^{2+}, and NH_4^+ (all at pL ≈ 5.4). The required volumes of H_2O- or D_2O-containing RNA, substrate, or buffer were mixed to obtain the required mole fraction (n) of D_2O. The mole fraction was varied from 0 to ∼1, with approximately 8−10 data points between these limits, with each experiment repeated at least twice. Calculations of the mole fraction took into account differences in the density of the two solvents, as described.[33,34,38]

The proton inventory plots were fit to the standard Gross−Butler equation, wherein the transition state fraction factors are assumed to be equal in the case of more than one transfer.[39]

$$\frac{k_n}{k_0} = (1 - n + n\Phi)^m \quad (5)$$

Here n is the mole fraction of D_2O, k_n is the observed rate at n mole fraction of D_2O, k_0 is the observed rate in 100% H_2O (n = 0), m is the number of protons transferred, and Φ is the transition state fractionation factor, which describes the preference of a given site for deuterium relative to a bulk water molecule.

For a reaction involving one proton transfer (i.e., m = 1), eq 5 simplifies to a linear equation wherein the plot of k_n/k_0 versus n will yield a slope of $\Phi - 1$ and a y-intercept of 1. For a reaction involving two proton transfers, the shape of the k_n/k_0 versus n plot is concave (bowl-shaped). Conversely plots of $(k_n/k_0)^{1/2}$ versus n are linear for a concerted two proton inventory (i.e., m = 2) but convex (dome-shaped) for a one-proton inventory.[39,40]

Calculation of Thio Effects. To quantify the effect a phosphorothioate substitution has on the rate, the thio effect can be calculated:

$$\text{thio effect} = k_O/k_S \quad (6)$$

where "k_O" is the observed reaction rate for the oxo substrate and "k_S" is the observed reaction rate for the stereospecific phosphorothioate substrate. As discussed in our earlier work, thio effects fall into three classes: normal thio effect (>1; i.e., oxo substrate reacts faster than the thio substrate), no thio effect (∼1; i.e., oxo and thio substrates react at similar rates), and an inverse thio effect (<1; i.e., thio substrate reacts faster than the oxo substrate).[19]

Molecular Dynamics (MD) Simulations. The classical MD simulations were performed using the DESMOND program[41] with the AMBER99 force field,[42] periodic boundary conditions, and the Ewald treatment of long-range electrostatics. The simulations were based on a modified precleaved crystal structure (PDB ID 3NKB).[37] The details of these modifications, which include modeling of the U-1 residue and the scissile phosphate, are described elsewhere.[31,43] This crystal structure had the cleavage site modeled after the hammerhead ribozyme.[37,44] Because modeling was required at the active site, the catalytic relevance of the structure required testing by experiments. Support for this structure has come from recent thiophosphate/rescue experiments[19] and mutants at the active site,[35] as well as a plethora of calculations and modeling from our laboratories[31,36,43,45,46] as well as others.[25−27] The R_P and S_P substrate starting structures were generated after mutating the appropriate nonbridging oxygen at the scissile phosphate to sulfur *in silico*.

The Accelrys Discover Studio Visualizer (version 2.0) software was used to add the hydrogen atoms for the entire system. Residues C41 and C75 were kept protonated to maintain critical hydrogen-bonding interactions and to allow C75 to function as a general acid.[43,45] These protonation states were chosen to maintain the active site geometry conducive to the self-cleavage reaction. Experimental data indicate that C75 is protonated at neutral pH in the absence of Mg^{2+} or in the presence of physiologically low (∼0.4 mM) Mg^{2+}.[6,34,47] C41 has mixed protonation at neutral pH, but, as indicated by MD simulations[45] and experiments,[47] its deprotonation does not significantly affect the active site.

The simulation box was prepared by immersing the ribozyme, along with its crystallographically resolved Mg^{2+} ions and water molecules, in an orthorhombic box containing rigid TIP3P water molecules. Appropriate quantities of Na^+ and Cl^- ions were added, first to neutralize the box and then to achieve a physiological salt concentration of 0.15 M. Note that the experiments were performed at a higher salt concentration, which would exert a long-range electrostatic effect but is not expected to qualitatively influence the local geometrical changes in the active site, although the impact is not known. A thorough

DOI: 10.1021/acs.biochem.5b00190
Biochemistry 2015, 54, 2160−2175

Table 1. Thio Effects in the WT HDV Ribozyme in the Presence of Monovalent Metal Ions[a]

M^+	ionic conditions (M)	oxo $k_O \times 10^5$ (min^{-1})[b]	R_P substrate $k_S \times 10^5$ (min^{-1})[b]	k_O/k_S[c]	S_P substrate $k_S \times 10^5$ (min^{-1})	k_O/k_S
Li^+	0.5	60 ± 11	8.65 ± 3.3	6.9 ± 2.9	24.1 ± 7.5	2.5 ± 0.9
	1	790 ± 120	15.0 ± 2.8	53 ± 13	112 ± 16	7.1 ± 1.5
	2	1350 ± 50	19.7 ± 2.1	69 ± 7.7	217 ± 6.0	6.2 ± 0.3
	3	2800 ± 150	22.0	130 ± 6.9	630 ± 14	4.4 ± 1.0
	4	4250 ± 200	27.5 ± 2.1	150 ± 14	925 ± 50	4.6 ± 0.3
Na^+[d]	0.5	0.37 ± 0.03	NA	NA	1.63 ± 0.04	1/(4.4 ± 0.4)
	1	1.10 ± 0.07	0.2	5.5 ± 0.4	5.20 ± 0.40	1/(4.7 ± 0.4)
	2	6.21 ± 1.1	0.16	39 ± 6.9	44.1 ± 6.8	1/(7.1 ± 1.7)
	3	11.7 ± 1.5	0.21	56 ± 7.1	62.2 ± 3.6	1/(5.3 ± 0.7)
	4	29.0 ± 7.2	0.27	110 ± 27	66.3 ± 2.1	1/(2.3 ± 0.6)
K^+[e] pH 5.5	0.25	0.14	NA	NA	0.80	1/5.7
	0.5	0.37	NA	NA	0.38	~1.0
	1	0.26	NA	NA	0.29	~1.0
NH_4^+	0.5	1.62 ± 0.18	NA	NA	13.8 ± 0.80	1/(8.5 ± 1.1)
	1	7.61 ± 1.1	0.90	8.4 ± 1.2	130 ± 28	1/(17 ± 4.4)
	2	15.3 ± 1.5	3.1 ± 0.8	4.9 ± 1.4	242 ± 14	1/(16 ± 1.8)
	3	16.5 ± 1.4	2.0 ± 0.3	8.2 ± 1.4	348 ± 31	1/(21 ± 2.6)
	4	15.0 ± 2.6	3.0 ± 1.0[f]	4.7 ± 1.7	255 ± 22	1/(17 ± 3.3)

[a] k_{obs} measured at 37 °C in 25 mM MES (pH 6.5), 100 mM Na_2EDTA for all conditions except K^+, which is in 25 mM MES (pH 5.5), 100 mM Na_2EDTA. [b] Error in k_0 and k_S is from the standard deviation of three or more experimental observations. The experiments where no error is reported were only done once. Note also that the actual rate constants should be calculated as the value shown divided by 10^5; for instance, the first entry is 60×10^{-5} min^{-1}. [c] Thio effect is the ratio k_O/k_S as defined in eq 6. Error is propagated from the relative errors.[68] Some thio effect values are written as 1/inverse value, and the inverse value is often quoted in the text. [d] The final concentration of Na^+ has another 0.2 M (not listed in table entries) owing to the presence of 0.1 M Na_2EDTA. All other reactions also have an addition of 0.2 M Na^+ from the EDTA. [e] The extent of reaction of the oxo substrate in the presence of KCl at pH > 6.0 was found to be slow. Decreasing the pH was found to increase the rate of reaction, as would be expected from an inverted rate−pH profile as found in the presence of Na^+. To measure reliable rates all the reactions in the presence of KCl were performed at pH 5.5. Higher concentrations of KCl inhibited the reaction to the point where a reliable rate could not be measured. [f] The R_P substrate exhibited background cleavage (0.2×10^{-5} min^{-1}) in the presence of 4 M NH_4Cl and absence of the ribozyme. The rate of background cleavage was subtracted from the observed rate to give the corrected value provided (see Materials and Methods). 'NA' is not available.

equilibration procedure, as described elsewhere, was performed prior to data collection.[43,46]

Quantum Mechanical/Molecular Mechanical (QM/MM) Free Energy Simulations. An interfaced version of Q-Chem[48] and CHARMM[49] was used to perform the QM/MM free energy simulations. The QM/MM description of the system employed in the current simulations is similar to that used in our previous studies. A schematic depiction of the reaction coordinates used in the string calculations is provided as Figure S2, Supporting Information.[31,36] The QM region consisted of 87 atoms and was treated with density functional theory (DFT) using the B3LYP functional[50] and the 6-31G** basis set, while the MM region was described by the AMBER99 force field.[42] The QM/MM boundary was treated using the standard link atom technique. The initial system was prepared as described above for the classical MD simulations. After an initial equilibration of only the solvent and monovalent ions, all water molecules and ions lying outside a distance of 20 Å from the ribozyme were deleted to reduce the size of the system and increase computational efficiency. The QM/MM trajectories were propagated using Langevin dynamics with 1 fs time step. During the simulations, all atoms lying outside a residue-based cutoff of 20 Å from the phosphorus atom of the scissile phosphate remained fixed. The O2′ of the U-1 residue was kept deprotonated to drive its nucleophilic attack on the scissile phosphate. The procedure for obtaining the initial pathways for the QM/MM free energy simulations was described in our previous work.[36]

The QM/MM free energy simulations were performed using an approach that combines umbrella sampling simulations with a finite temperature string method,[51] as in our previous study.[36] In this approach, the reaction pathway is approximated as a "string", which is a curve in the multidimensional space of only the relevant reaction coordinates. The string is divided into a series of images, where each image corresponds to certain values of the reaction coordinates. In our implementation, for each iteration 100 fs of umbrella sampling was performed for each image with restraining potentials applied to the chosen reaction coordinates. The average values of the reaction coordinates were calculated from the MD trajectories, and the string was updated by fitting the average reaction coordinates to a new curve. This process of updating the string after each iteration was continued until the string was converged according to previously defined criteria.[36] The umbrella sampling data from all of the iterations were then unbiased using the multidimensional weighted histogram analysis method (WHAM) to generate the multidimensional free energy surface of the reaction. The converged string corresponds to the minimum free energy path (MFEP) of the reaction on that multidimensional free energy surface. The convergence threshold used for the WHAM iterations was 0.001 kcal/mol.

We utilized this method to investigate the cleavage mechanism of the R_P and S_P phosphorothioate substrates in the presence of either a Mg^{2+} ion or a Na^+ ion at the catalytic position. In total, we performed four independent sets of QM/MM free energy simulations to study the following four scenarios: (A) R_P substrate with a Mg^{2+} ion at the active site, (B) S_P substrate with a Mg^{2+} ion at the active site, (C) R_P substrate with a Na^+ ion at the active site, and (D) S_P substrate with a Na^+ ion at the active site. The initial string in each case corresponded to a sequential mechanism, in which the reaction

DOI: 10.1021/acs.biochem.5b00190
Biochemistry 2015, 54, 2160−2175

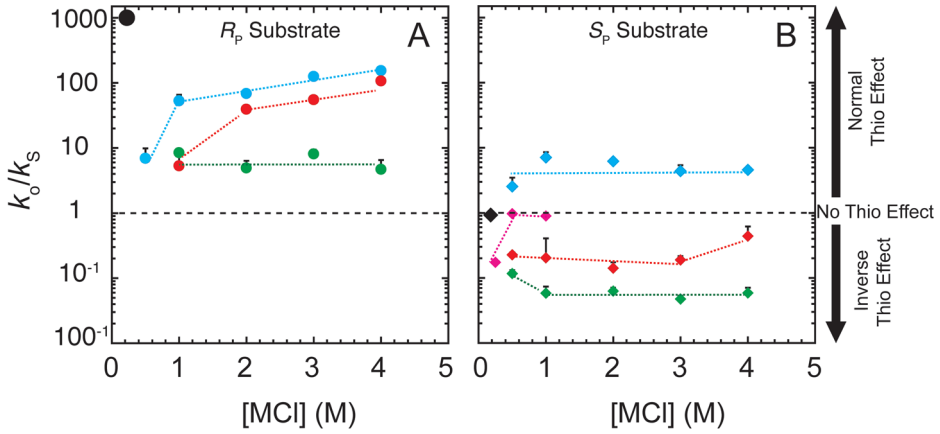

Figure 2. Dependence of thio effect on monovalent ion identity and concentration. Symbols are as follows: Li^+: cyan; Na^+: red; NH_4^+: green; K^+: pink; 10 mM Mg^{2+}: black single point. Thio effects for the (A) R_P (circle) substrate and (B) S_P (diamond) substrate. Thio effects in the presence of 10 mM Mg^{2+}, ~1000 for R_P slow phase of substrate and 0.97 for S_P substrate, are from an earlier study.[19] No rates could be obtained for the R_P substrate in the presence of KCl, where the extent of cleavage for the reaction was the same as the background cleavage. The dashed black line denotes the point of no thio effect, where $k_O = k_S$; data above the dashed line lie in the normal thio effect region $k_O > k_S$, whereas the data below the line lie in the inverse thio effect region $k_O < k_S$. The trend lines are only to guide the eye.

passes through a thiophosphorane intermediate and was constructed from interpolation between representative structures along the pathway. Twelve active site interatomic distances were chosen as reaction coordinates, and restraining potentials with a force constant of 100 kcal mol^{-1} A^{-2} were used for the umbrella sampling simulations. In each case, the reaction pathway was represented by 21 images, and the evolution of the string was preceded by 150 fs of QM/MM equilibration with harmonic restraints acting on all reaction coordinates. The total simulation times for sets A, B, and D was 45 ps, and for set C was 56 ps.

Because the conformational sampling is limited for these QM/MM free energy simulations, we performed a statistical analysis to examine convergence, as described in the Supporting Information (Table S1). On the basis of this analysis, we estimated the error in the free energy barriers due to statistical fluctuations to be ~0.8 kcal/mol. This estimate does not include systematic errors due to limitations of DFT, including the functional and basis set, and the molecular mechanical force field. Furthermore, in prior work,[36,52] we have shown that these types of QM/MM simulations do not depend strongly on the initial string. Specifically, we performed calculations for two different initial strings associated with distinct mechanisms (i.e., concerted and sequential) and showed that the two calculations resulted in the same mechanism with similar free energy barriers. This test was performed for both the HDV and the *glmS* ribozyme reactions.

Classical Free Energy Simulations. The approach of combining umbrella sampling simulations with a finite temperature string method was also employed to calculate the free energy difference between the two states shown in Figure S3, Supporting Information to determine their relative populations in the absence of the active site Mg^{2+}. Because no chemical bonds are broken or formed, the entire system was described by the AMBER99 classical force field.[42] The initial string was generated from a linear interpolation connecting the two end states depicted in Figure S3. The reaction coordinates considered in these simulations were the angles U-1(O2′):U-1(HO2′):G1(O1P) and U-1(O2′):U-1(HO2′):G28(O2′), as defined in Figure S3, and the string was represented by 31 images. We performed 100 ps of MD on each image per iteration, and the simulations were converged after 15 iterations, corresponding to a total simulation time of 46.5 ns.

RESULTS

A Periodic Trend of Thio Effects in Monovalent Ions Alone. We began by investigating the effect of various monovalent ions on the reactivity of the two stereopure thio substrates. In the case of the HDV ribozyme, catalysis can occur in the absence of divalent ions, albeit at a much slower rate.[6,7,34] The presence of 100 mM EDTA in the present experiments ensured no influence from any divalent metal ion contamination (see Materials and Methods). Thio effects for the R_P substrate were measured in Li^+, Na^+, and NH_4^+, with ion concentrations ranging from 0.5 to 4 M (Table 1, Figure 2A).[c]

Normal thio effects were observed for the R_P substrate in the presence of all three monovalent ions (Table 1). Maximal normal thio effects of ~100-fold were observed in the presence of 4 M Li^+ and 4 M Na^+ (Figure 2A, cyan and red circles). Moreover, these effects were monovalent ion concentration dependent: the thio effect increased ~20-fold in Li^+ and Na^+ upon increasing concentration from 0.5 or 1 M up to 4 M (Figure 2A). This increase is primarily due to an increase in the rate of the oxo substrate (Figure S4A; compare cyan squares to circles, and red squares to circles). In particular, upon increasing the Li^+ concentration from 0.5 to 4 M, the rate of the oxo substrate increased by ~70-fold (Figure S4A, cyan squares), while the rate of the R_P substrate increased by only ~3-fold (Figure S4A, cyan circles). Likewise, upon increasing the Na^+ concentration from 1 to 4 M, the rate of the oxo substrate increased by ~30-fold (Figure S4A, red squares), while the rate of the R_P substrate increased by only ~1.3-fold (Figure S4A, red circles).

In the presence of NH_4^+, however, the normal thio effects for the R_P substrate were relatively modest, at ~5−8-fold (Table 1). Moreover, unlike in Li^+ and Na^+, the normal thio effects in NH_4^+ did not show a strong dependence on ion concentration over the range of 0.5−4 M (Figure 2A, green circles). This observation suggests that low charge density ions may play a different role in the mechanism, even at very high concentrations, than higher charge density ions.

DOI: 10.1021/acs.biochem.5b00190
Biochemistry 2015, 54, 2160−2175

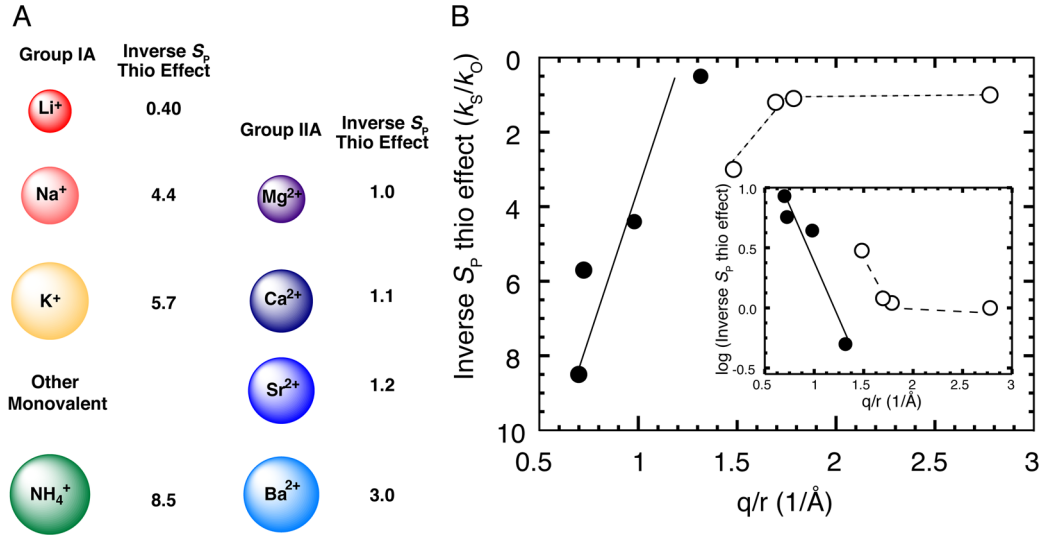

Figure 3. Trend of the S_P inverse thio effect. (A) Group IA and IIA metal ions and their respective inverse thio effects. The size of the spheres reflects the relative sizes of the dehydrated ions. For monovalent ions, the inverse thio effects provided are for the lowest concentration of ions: 0.25 M K^+, 0.5 M Li^+, 0.5 M Na^+, and 0.5 M NH_4^+ (Table 1). Divalent ions were present at 10 mM (Table 2). (B) Plot of inverse S_P thio effect versus the ratio of ionic charge and ionic radius.[66,69,70] Monovalent ions are shown in closed circles and divalent ions in open circles. Inset: logarithm of the inverse S_P thio effect versus the ratio of ionic charge to ionic radius, which suggests a linear energy relationship.

Table 2. Thio Effects in the WT HDV Ribozyme in the Presence of Divalent Metal Ions[a]

10 mM M^{2+}	ionic radii (pm)[b]	oxo k_O (min^{-1})	S_P substrate k_S (min^{-1})[c]	k_O/k_S[d]
Mg^{2+}	72	1.16 ± 0.13	1.20 ± 0.07	~1/(1.0 ± 0.1)
Ca^{2+}	112	0.72 ± 0.06	0.79 ± 0.10	~1/(1.1 ± 0.2)
Sr^{2+}	118	0.013 ± 0.005	0.015 ± 0.0003	~1/(1.2 ± 0.5)
Ba^{2+}	135	0.0021 ± 0.00017	0.0058 ± 0.00014	~1/(3.0 ± 0.2)

[a] k_{obs} measured at 37 °C in 50 mM NaMES (pH 5.6). [b] Dehydrated ionic radii for divalent metal ions obtained from refs 66 and 69. [c] Errors in k_0 or k_S is the range of two experimental observations. [d] Thio effect is the ratio k_O/k_S as defined in eq 6. Error is propagated from the relative errors.[68] Some thio effect values are written as 1/inverse value, and the inverse value is often quoted in the text.

Thio effects for the S_P substrate were similarly measured in Li^+, Na^+, K^+, and NH_4^+, with ion concentrations again ranging from 0.5 to 4 M (Table 1, Figure 2B). A normal thio effect was observed only in Li^+, and a modest one at that, with a weak dependence on Li^+ ion concentration (Figure 2B, cyan diamonds) and a maximal value for the normal thio effect of 7.1 ± 1.5-fold at 1 M Li^+.

In contrast to Li^+, the other three monovalent ions gave *inverse* thio effects for at least a portion of their concentration profiles. Maximal inverse values for the S_P substrate of (7.1 ± 1.7)- and 5.7-fold were found in 2 M Na^+ and 0.25 M K^+, respectively (Table 1, Figure 2B, red and pink diamonds). Upon increasing the concentration of Na^+ to 4 M, the inverse S_P thio effect was nearly gone (Figure 2B, red diamonds), similar to the S_P no thio effect in 10 mM Mg^{2+} (Figure 2B, black diamond).[19] Increasing the concentration of K^+ to 0.5 or 1 M also reduced the inverse thio effect to unity (Figure 2B, pink diamonds). Overall, the thio effects observed in high concentrations of group IA metal ions are generally trending toward those for 10 mM Mg^{2+} for both the R_P and S_P substrates (Figure 2A,B, compare black symbol to cyan, red, and pink symbols).

The largest inverse thio effects for the S_P substrate were observed in the presence of NH_4^+ of 9–21-fold (Table 1). As with the R_P normal thio effects in NH_4^+, the inverse S_P thio effects in NH_4^+ did not show a strong dependence on NH_4^+ concentration over the range of 1–4 M (Figure 2). The large magnitude of inverse thio effect in NH_4^+ may be a result of NH_4^+ participating in one of the proton transfers involving C75 as well as its inability to stabilize a phosphorane dianion (see Discussion).

Figure 3 depicts the magnitude of the inverse S_P thio effect versus q/r, where q is the ionic charge and r is the ionic radius. For monovalent ions, the data obey a semilogarithmic linear relationship suggestive of a linear energy relationship (Figure 3B, inset), with the biggest inverse thio effect for those ions with the lowest charge density.

Thio Effects in Divalent Ions. Divalent ions are known to play important roles in HDV ribozyme catalysis. As discussed above, we observed a semilogarithmic trend in the inverse thio effects with increasing ionic charge/ionic radius ratio (q/r) in monovalent ions (Figure 3). In a similar light, the effect of q/r on the thio effect was investigated for divalent ions (Table 2). For divalent ions, we opted to focus on alkaline earth metal ions because they have similar properties to each other. Transition metals were not used because they can interact with the nucleobases in special ways, for example, through the Hoogsteen face,[53−55] and Mn^{2+} and Cd^{2+} were previously studied.[19] The rate for the oxo substrate was found to be fastest in the presence of Mg^{2+} (1.2 ± 0.1 min^{-1}) and slowest in the presence of Ba^{2+} (0.002 ± 0.0002 min^{-1}), which agrees with previous one-piece HDV ribozyme trends,[56] although the rates of the reaction are somewhat slower in the two-piece construct.[19,35]

Thio effects were measured in Mg^{2+}, Ca^{2+}, Sr^{2+}, and Ba^{2+} for the S_P substrate (Table 2). In the presence of Mg^{2+}, no S_P thio

DOI: 10.1021/acs.biochem.5b00190
Biochemistry 2015, 54, 2160–2175

effect was found, similar to previously reported results on the genomic and antigenomic ribozymes.[19,57] Negligible inverse thio effects of 1.1 ± 0.2 and 1.2 ± 0.5 were found in Ca^{2+} and Sr^{2+}, respectively, revealing no significant dependence of inverse thio effect on the ionic radius of divalent metal ions over this range of ion size. A significant inverse thio effect of 3.0 ± 0.2 was found in Ba^{2+}, however, consistent with its significantly larger ionic radius of 135 pm and lower charge density (see Discussion). These data are plotted in Figure 3 as inverse S_P thio effect versus q/r, alongside the monovalent ion data.

Classical MD Trajectories and Classical Free Energy Simulations on U-1−2′-OH Interactions. We next conducted classical and quantum mechanical calculations to probe the molecular origin of the inverse thio effects with low charge density ions. This subsection describes the classical calculations, and the next subsection describes the quantum calculations. One possible origin of the inverse thio effect with low charge density ions is relief of a putative hydrogen bond between the 2′-OH of U-1 and the *pro*-S_P oxygen, which we refer to as "Model 1" or the "Hydrogen-Bonding Effect Model" (Figure 4). Breaking of this hydrogen bond would free up the 2′-OH to be deprotonated and then attack the scissile phosphate. To test this model, we inspected classical MD trajectories from our previous work,[43,45,46] monitoring the two O2′--HO2′---O(P) angles, as well as HO2′--O(P) distances, where O(P) denotes either of the two nonbridging oxygen atoms and HO2′ denotes the hydrogen of the 2′-OH of U-1. Presence of a hydrogen bond between the 2′-OH of U-1 and one of the nonbridging oxygen atoms was inferred when the O2′--HO2′--O(P) angle was 160−180° and the corresponding HO2′--O(P) distance was less than 2 Å. This 2′-OH−scissile phosphate interaction was explored via two simulations: (1) a Mg^{2+} ion at the catalytic site, and (2) a Na^+ ion at the catalytic site. For case (2), the Mg^{2+} ion at the catalytic site was removed and compensated by two Na^+ ions in the bulk, where Na^+ ions moved into the region of the active site during equilibration. In each case, two independent 25 ns trajectories were inspected.[43,45,46] An important feature of the active site of the HDV ribozyme is the G25·U20 reverse wobble that interacts with the catalytic Mg^{2+} ion.[35,37] Previous experimental studies have found that the G25·U20 reverse wobble may be affected by changes in the ionic conditions.[58,59] In our calculations, no significant conformational changes in the G25·U20 reverse wobble were observed between monovalent and divalent ions. Previous theoretical studies from our group have shown that the reverse wobble remains intact in the presence or absence of divalent metal ions when C75 is protonated.[43]

The O2′--HO2′--O(P) angles and HO2′--O(P) distances for the MD trajectories with Mg^{2+} or Na^+ at the catalytic site are provided in Figure S5, Supporting Information. In the presence of an active site Mg^{2+} (Figure S5, red and blue), the two trajectories behave similarly. The O2′--HO2′--*pro*-R_P oxygen and O2′--HO2′-*pro*-S_P oxygen angles are at nonoptimal values of ∼50° and ∼70°, respectively, while the HO2′--*pro*-R_P oxygen and HO2′--*pro*-S_P oxygen distances are also at nonoptimal values of ∼3.5 Å. These angles and distances suggest that there is no hydrogen bonding between 2′-OH and the scissile phosphate in the presence of the active site Mg^{2+} ion.

In the absence of the active site Mg^{2+} ion, the two MD trajectories behave quite differently. In one trajectory (Figure S5, magenta), there are acute O2′--HO2′-*pro*-R_P oxygen and O2′--HO2′-*pro*-S_P oxygen angles of less than 40°, as well as very long HO2′--*pro*-R_P oxygen and HO2′--*pro*-S_P oxygen distances of ∼6 Å. The other trajectory (Figure S5, green), however, is suggestive of hydrogen bonding between the 2′-OH of U-1 and the scissile phosphate. A 2′-OH--*pro*-S_P oxygen interaction is observed at ∼9 ns and persists for the remaining ∼16 ns of the simulation; this interaction is supported by an O2′--HO2′-*pro*-S_P oxygen angle of ∼160° and an HO2′--*pro*-S_P oxygen distance of ∼1.7 Å. This observation suggests that a hydrogen bond between the 2′-OH of U-1 and the *pro*-S_P oxygen is possible. According to this model, the inverse S_P thio effect would arise from the breaking of this inhibitory hydrogen bond, which would allow deprotonation of the 2′-OH and subsequent nucleophilic attack on the scissile phosphate (Figure 4, compare panel F to panels D and E). However, we also note that in this same trajectory (Figure S5, green) when the 2′-OH of U-1 does not interact with the *pro*-S_P oxygen, it interacts with the *pro*-R_P oxygen with ideal hydrogen bonding angles and distances, albeit for somewhat less time (Figure S5, green).

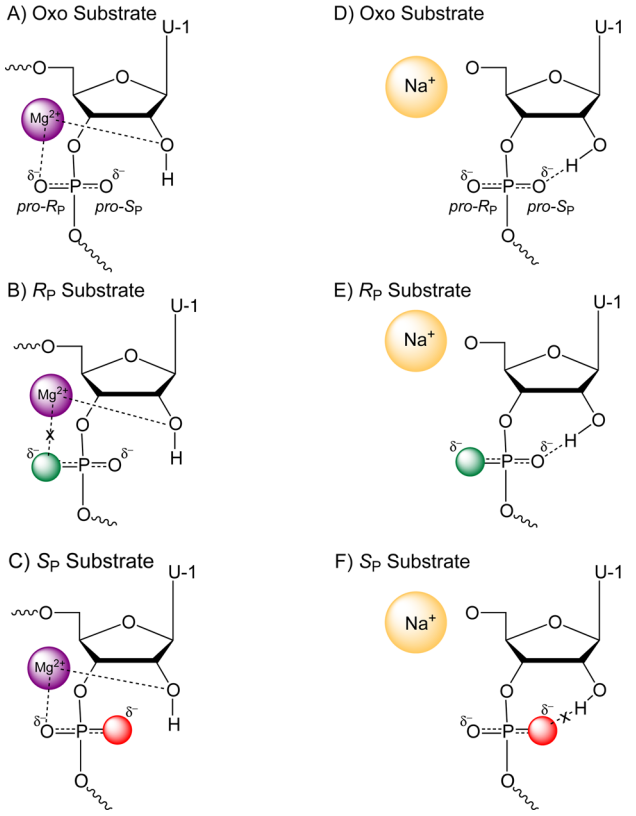

Figure 4. Interaction between the 2′-OH of U-1 and *pro*-S_P oxygen atom of the scissile phosphate in the presence of various metal ions that leads to the hydrogen-bonding effect model. Panels A−C are in the presence of the catalytic Mg^{2+} ion for the oxo, R_P, and S_P substrates, respectively. The 2′-OH of U-1 is depicted as not interacting with the S_P position due to its interaction with Mg^{2+} as revealed by a crystal structure and rate−pH profiles.[6,37] The normal thio effect for the R_P substrate[19] arises from loss of the catalytic Mg^{2+} interaction in the R_P substrate, depicted with an "x" in panel B. Panels D−F are in the presence of diffusely bound Na^+ for oxo, R_P, and S_P substrates, respectively. The 2′-OH interacts with the *pro*-S_P oxygen in the oxo and R_P substrates, whereas the sulfur at the *pro*-S_P position for the S_P substrate destabilizes this interaction. The absence of the inhibitory hydrogen bond, depicted with an "x", could possibly result in an inverse thio effect for the S_P substrate in Na^+. The *pro*-R_P and *pro*-S_P oxygen atoms are shown in green and red, respectively.

DOI: 10.1021/acs.biochem.5b00190
Biochemistry 2015, 54, 2160−2175

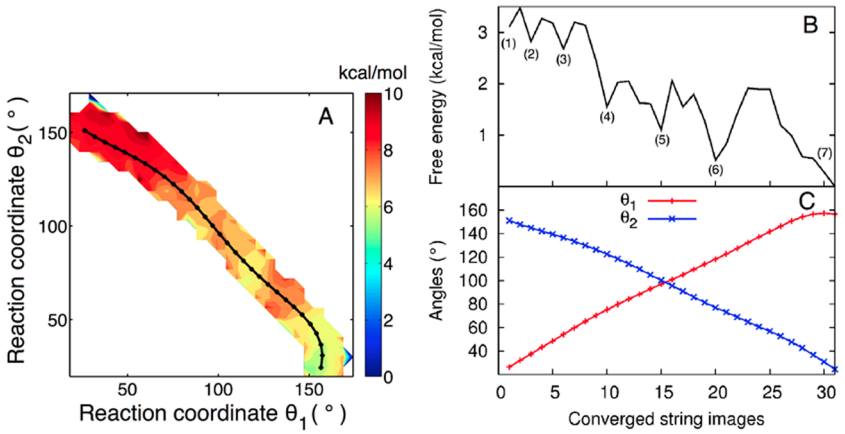

Figure 5. Free energy simulation for U-1 2′-OH interactions in the absence of the active site Mg^{2+}. (A) The two-dimensional free energy surface obtained from the free energy simulations, where the two angle reaction coordinates are defined in Figure S3, and the black curve denotes the converged MFEP. This figure illustrates the conversion between the two states depicted in Figure S3, indicating that the most favorable orientation of U-1(HO2′) is the one in which it hydrogen bonds to the *pro*-S_P oxygen of the scissile phosphate. (B) The one-dimensional free energy profile along the converged MFEP. Representative structures corresponding to the various minima along the MFEP are depicted in Figure S6. All of these configurations are thermodynamically similar and are expected to be populated at room temperature. Note that the free energies of the configurations with U-1(HO2′) hydrogen bonded to the *pro*-R_P or *pro*-S_P oxygen differ by only ∼0.5 kcal/mol. (C) Values of the reaction coordinates along the MFEP.

The conformational sampling in these MD trajectories is not sufficient to obtain reliable statistics about these hydrogen-bonding interactions. Thus, we also performed free energy simulations using umbrella sampling methods to obtain more reliable relative free energies among configurations with different orientations of the 2′-OH of U-1 in the absence of the active site Mg^{2+}. Specifically, umbrella sampling simulations with the finite temperature string method were used to transform between a state in which the 2′-OH of U-1 hydrogen bonds to the 2′-OH of G28 and a state in which the 2′-OH of U-1 hydrogen bonds to the *pro*-S_P oxygen on the scissile phosphate (Figure S3). As no forming or breaking of chemical bonds was involved, the transformation was described entirely by a classical force field. The two-dimensional free energy surface for the transformation is shown in Figure 5A, and the one-dimensional free energy profile along the MFEP is shown in Figure 5B. The initial and final states are provided in Figure S3, and snapshots of the active site corresponding to the various minima observed in Figure 5B are provided in Figure S6.

On the basis of the relatively small free energy barriers connecting the various minima in Figure 5B, they are all expected to be populated at room temperature. The landscape along these angular coordinates appears to be relatively flat, thereby enabling the sampling of many thermodynamically similar conformations. Interestingly, state (6), which corresponds to the penultimate minimum, has the 2′-OH of U-1 hydrogen bonded to the *pro*-R_P oxygen, rather than the *pro*-S_P oxygen. State (6) has nearly identical free energy to state (7), which is the lowest minimum, with the 2′-OH of U-1 hydrogen bonded to the *pro*-S_P oxygen.

QM/MM Free Energy Simulations for the R_P and S_P Substrates in the Presence of Mg^{2+} or Na^+. A second possible origin of the inverse thio effect with low charge density ions is facilitation of the stepwise mechanism by virtue of having a sulfur at the *pro*-S_P position, which we refer to as "Model 2", or the "Cleavage Effect Model". We tested this model by carrying out calculations using a QM/MM approach (this subsection) and performing experiments using proton inventories and rate−pH profiles (next subsection). As mentioned, prior experimental and theoretical studies support a model in which the reaction occurs via a sequential mechanism in the presence of Na^+ and a concerted mechanism in the presence of Mg^{2+}.[33,34,36] To test this model, we carried out QM/MM free energy simulations to obtain an MFEP for the cleavage of the R_P and S_P substrates with a Mg^{2+} ion at the catalytic site or with a Na^+ ion rather than a Mg^{2+} ion at the catalytic site. For the latter case, the Mg^{2+} ion at the catalytic site was removed, and two Na^+ ions were placed in the bulk solvent prior to equilibration; during equilibration, Na^+ ions moved into the region of the catalytic site. As discussed previously, the Mg^{2+} ion exhibits a chelated interaction, while the Na^+ ion exhibits a diffuse interaction, at the catalytic site.[43]

The QM/MM free energy simulations were performed as described previously,[36] except that the appropriate nonbridging oxygen at the scissile phosphate was replaced with sulfur. We first consider reactions of the R_P, S_P, and oxo substrates in Mg^{2+}. In the presence of the active site Mg^{2+} ion, the R_P substrate was found to undergo cleavage via a dianionic thiophosphorane-like transition state (Figure S7). This pathway is similar to that of the oxo substrate in the presence of the active site Mg^{2+} ion; however, the free energy barrier was much higher for the R_P substrate than the oxo substrate (21.7 versus 12.8 kcal/mol). The higher free energy barrier agrees qualitatively with our recent experiments, wherein a large normal thio effect was found for the R_P substrate in the presence of Mg^{2+} (∼1000-fold).[19]

Similar to the R_P and oxo substrates with an active site Mg^{2+} ion, the S_P substrate in the presence of the active site Mg^{2+} was found to undergo catalysis via a dianionic thiophosphorane-like transition state (Figure S8). The free energy barrier was the same as that for the oxo substrate (12.7 kcal/mol), which agrees with our recent experiments wherein the oxo and the S_P substrates reacted at similar rates in the presence of Mg^{2+}.[19] An overlay of the QM/MM free energy simulations for the R_P, S_P, and oxo substrates in the presence of Mg^{2+} is provided in Figure 6A, which emphasizes the similarity of the free energy

DOI: 10.1021/acs.biochem.5b00190
Biochemistry 2015, 54, 2160−2175

profiles of the oxo and S_P substrates, and the higher barrier of the R_P substrate.

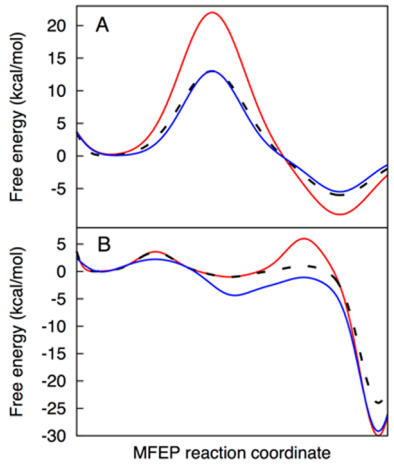

Figure 6. Schematic illustration of the one-dimensional free energy profiles along the MFEPs of the oxo (black, dashed curve) substrate, and R_P (red curve) and S_P (blue curve) phosphorothioate substrates in the presence of either a Mg^{2+} ion (A) or a Na^+ ion (B) at the catalytic site. These curves represent interpretation of the data according to Model 2 of the Discussion. The curves were constructed by fitting the respective raw data to a linear combination of three to five Gaussian functions. The raw data obtained from QM/MM free energy simulations are provided in Figures S7–S10 for the R_P and S_P substrates and in Figures 4 and 7 in ref 36 for the oxo substrates. In each panel, the maxima and minima of the three curves are aligned to have approximately the same MFEP reaction coordinates by scaling the *x*-axes of the curves to facilitate visualization. The *y*-axes are not scaled, however, to retain the calculated relative free energies for all of the curves.

Next we consider reactions of the R_P, S_P, and oxo substrates in Na^+. In the presence of Na^+ instead of Mg^{2+} at the catalytic site, the R_P substrate was found to undergo cleavage via a thiophosphorane intermediate (Figure S9). The reaction pathway is again similar to that of the oxo substrate under the same ionic conditions, with a more modestly increased free energy barrier for the second step of the R_P substrate (first and second barriers of ~3.5 and ~2 kcal/mol for the oxo substrate versus ~3.5 and ~7 kcal/mol for the R_P substrate). These results also corroborate our experimental measurements, wherein a normal thio effect is found for the R_P substrate in the presence of Na^+ (Figure 2).

In the presence of Na^+ at the active site, the S_P substrate also undergoes reaction via a thiophosphorane intermediate (Figure S10), similar to the oxo (phosphorane intermediate) and R_P (thiophosphorane intermediate) substrates under the same ionic conditions (Figure S9). However, the free energy profile in the presence of Na^+ is altered in the presence of the S_P substrate compared to the oxo substrate. The first free energy barrier is lower for the S_P substrate than for the oxo substrate (~2 and ~3.5 kcal/mol, respectively). The reaction is downhill from the thiophosphorane and phosphorane intermediates for both the S_P and oxo substrates, respectively, and the pre-equilibrium for 2′-OH deprotonation is expected to combine with the free energy barrier for the phosphorane intermediate formation, as described previously.[36] We note that the 2′-OH activation pre-equilibrium is not expected to be significantly affected by the thio substitution according to Model 2, which accounts for the inverse thio effect not by breaking of an inhibitory hydrogen bond between the 2′-OH of U-1 and the scissile phosphate, but by facilitation of a stepwise mechanism owing to a more electrophilic phosphorus as described below. Thus, for the purposes of analysis by Model 2, we neglect any thio effect on the pre-equilibrium constant, and the free energy barriers of the first step in the cleavage mechanism for the thio and oxo substrates can be compared directly.[d] A difference of ~1.5 kcal/mol in the first free energy barrier between the S_P and oxo substrates is consistent with the inverse thio effect of ~3–20-fold that we observed in the presence of low charge density ions. This observation suggests that Model 2, within the ~1 kcal/mol statistical error limits of the calculations, provides a possible explanation for the inverse thio effects (see Discussion). An overlay of the QM/MM free energy simulations for the R_P, S_P, and oxo substrates in the presence of Na^+ is provided in Figure 6B, which illustrates that the first barrier is lower for the S_P substrate than for the oxo substrate and that the second barrier is higher for the R_P substrate than for the oxo substrate.

Rate–pH Profiles and Proton Inventory Studies in the Presence of Li^+, NH_4^+, and Ba^{2+}. Calculations in the presence of Na^+, which has an inverse S_P thio effect, suggested that the reaction pathway is similar—stepwise with a phosphorane intermediate—in the presence of oxo, R_P and S_P substrates, but the relative heights of the free energy barriers are different. We next used experiments to test whether other ions, some of which also have inverse S_P thio effects, also favor a stepwise mechanism, and we compare these to prior experiments in Na^+. If so, this would provide a possible connection between an inverse S_P thio effect and a stepwise mechanism. We used the oxo substrate and Li^+, NH_4^+, and Ba^{2+} ions to perform proton inventory experiments, which detect the number of protons in flight in the rate-limiting step.[39] Prior proton inventory experiments from our lab conducted in the presence of Mg^{2+} and Na^+ gave inventories of 2 and 1, which supported concerted and stepwise mechanisms, respectively.[33,34] These findings were consistent with outcomes from prior QM/MM calculations,[36] as mentioned above.

Among the monovalent ions tested, only Li^+ gave a normal S_P thio effect, with a magnitude of 2–7-fold (Table 1). In contrast, NH_4^+ gave the largest inverse S_P thio effect among monovalent ions, with a magnitude of 8–20-fold (Table 1), while Ba^{2+} gave the only significant inverse S_P thio effect among divalent ions, with a magnitude of 3-fold (Table 2). In an attempt to correlate thio effects with a stepwise reaction pathway, we measured proton inventory experiments in the presence of 1 M Li^+, 10 mM Ba^{2+}, and 3 M NH_4^+.

Before carrying out the proton inventories, rate–pH profiles were measured. This was done for two reasons: (1) to find the plateau region of the profile in which to conduct the proton inventories, as undesired changes in rate due to known effects of D_2O on pK_a are minimized in the plateau region,[39] and (2) to test for inversion of the rate–pH profile because compared to Mg^{2+} the rate–pH profile in Na^+ is inverted, which is consistent with an indirect, noncatalytic role of Na^+ in the mechanism.[6,34] In the presence of 1 M Li^+, 10 mM Ba^{2+}, and 3 M NH_4^+ the rate pH–profiles are all inverted, with near log–linear decreases in the rate between pH 6.0 and 8.0 (Figure 7A). The inverted nature of these rate–pH profiles is similar to that observed in the presence of Na^+ suggestive of similar mechanisms. The pK_a's in the presence of Li^+, Ba^{2+}, and NH_4^+ are 6.3, 5.9, and 5.7, respectively. On the basis of the rate–pH

DOI: 10.1021/acs.biochem.5b00190
Biochemistry 2015, 54, 2160–2175

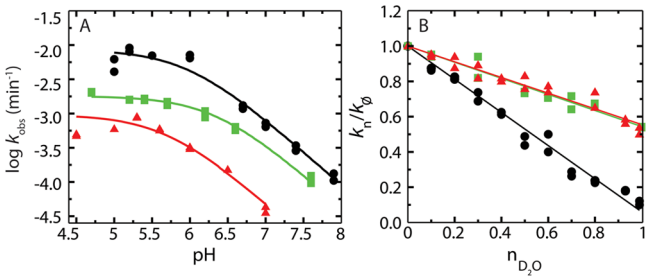

Figure 7. Rate–pH profiles and proton inventories in the presence of Li^+, Ba^{2+}, and NH_4^+. (A) Rate–pH profile in the presence of 1 M Li^+ (black circles), 10 mM Ba^{2+} (green squares), and 3 M NH_4Cl (red triangles). The pK_a's, obtained by fitting each data set to the logarithm of eq 3, were found to be 6.3, 5.9, and 5.7 in the presence of Li^+, Ba^{2+}, NH_4^+, respectively; the data point for NH_4^+ at pH 4.5 was excluded from the fit owing to the possibility of acid denaturation. A pL of 5.4 was chosen for the proton inventory studies as it lies in the plateau region of the rate–pH profile for all three ions. (B) Proton inventories in the presence of 1 M Li^+ (black circles), 10 mM Ba^{2+} (green squares), and 3 M NH_4^+ (red triangles) at pL 5.4. Each proton inventory was fit to a standard Gross-Butler equation for a single proton transfer as described in eq 5 (Li^+, black line; Ba^{2+}, green line; NH_4^+, red line). The transition state fractionation factor Φ was found to be 0.06 for Li^+, 0.54 for Ba^{2+} and 0.55 for NH_4^+, giving isotope effects of 17-fold, 1.9-fold, and 1.8-fold, respectively. The *R*-values for the fits to the Gross-Butler equation for a one-proton model were very good at 0.99 for Li^+, 0.98 for Ba^{2+}, and 0.97 for NH_4^+. The measurements were performed in duplicate and are plotted in the figure. A two-proton inventory can be ruled out for Li^+ by means of a square root plot[40] (see Figure S11). For Ba^{2+} and NH_4^+ the data fit equally well to a two-proton model with equivalent transition state fractionation factors (not shown), but a one-proton model is favored on the basis of parsimony. Such conclusions were made previously for similar types of plots.[34]

profiles, the proton inventory experiments in 1 M Li^+, 10 mM Ba^{2+}, and 3 M NH_4Cl were conducted at pL 5.4 because this lies in the plateau region of the inverted rate-pH profile for all three ions.

The proton inventory plots in the presence of Li^+, NH_4^+, and Ba^{2+} are provided in Figure 7B. In all three cases, plots of relative rate constants versus D_2O fraction (n) are linear, which is consistent with a one-proton inventory. Fractionation factors of 0.06, 0.55, and 0.54 (Figure 7B), corresponding to solvent isotope effects of 17-fold, ~2-fold, and ~2-fold, were found for Li^+, NH_4^+, and Ba^{2+} respectively. The proton inventories of unity and the inverted rate–pH profiles suggest that the mechanism proceeds via a stepwise proton-transfer catalyzed pathway in the presence of all three metal ions.[34] In the case of NH_4^+ and Ba^{2+}, which have inverse S_P thio effects, this correlation suggests that an inverse S_P thio effect is related to a stepwise pathway. For Li^+, which has an inventory of unity and an inverted rate–pH profile but a *normal* S_P thio effect, there may be no interaction between the very hard Lewis acid Li^+ and the soft Lewis base $S^{\delta-}$ that leads to a normal S_P thio effect despite the stepwise pathway (see Discussion).

Dual Rescue by Imidazole and NH_4^+. As mentioned above, the QM/MM results are consistent with an S_P sulfur atom lowering the first free energy barrier in the stepwise mechanism by ~1.5 kcal/mol, which is consistent with the inverse thio effects observed herein. However, we consistently observed larger inverse thio effects for NH_4^+ than the group IA monovalent ions at their lower concentrations (15–20-fold versus 4–7-fold, respectively). Because NH_4^+ has the potential to act as an acid/base catalyst, we considered the possibility that it might aid the reaction via proton transfer.

In the stepwise model, C75 may donate a proton from its exocyclic amine (N4) to the *pro*-R_P oxygen (Figure 1, lower pathway); it later accepts the *pro*-R_P proton back to its N4 and donates the proton from its N3 to the leaving group.[36] To test whether NH_4^+ could act as a surrogate for the N4 amine, we utilized the C75 deletion (C75Δ) mutant of the HDV ribozyme. In the presence of Mg^{2+}, the inactive C75Δ is known to be rescued by exogenous imidazole (up to 200 mM).[24,60]

Imidazole rescue of C75Δ was attempted in the presence of 1 M Na^+ and 100 mM Na_2EDTA for the WT oxo substrate, with the results summarized in Table S2. We found no reaction of C75Δ in the presence of 1 M Na^+, alone or even with 1 M imidazole.[e] In the presence of 1 M NH_4^+, again no reaction was found. However, upon addition of both 1 M imidazole and NH_4^+, reactivity was restored, albeit slowly ($k_{obs} \approx 10^{-5}$ min^{-1}).[f] In sum, imidazole together with ammonium rescue the activity of the C75Δ ribozyme in the absence of Mg^{2+} ions, suggestive of a more active role for NH_4^+ in the reaction than for other monovalent ions, possibly via proton transfer in the absence of divalent ions.

Thio effect studies were also carried out in the C75Δ mutant in the background of 1 M imidazole and 1 M NH_4Cl for both the R_P and the S_P substrate. The R_P substrate showed no detectable cleavage for up to 4 days, consistent with the continued importance of this atom, and thus relevance to the wild-type mechanism. A modest inverse S_P thio effect of 1.3-fold was observed for the C75Δ ribozyme in 1 M NH_4^+ and 1 M imidazole (Table S2).

DISCUSSION

The HDV ribozyme self-cleaves the phosphodiester bond between U-1 and G1 via attack of the 2′-OH on the scissile phosphate. Prior experiments indicate that this reaction can proceed by multiple channels, involving divalent ions or monovalent ions alone.[16] Prior calculations support the divalent ion channel as proceeding via a concerted metal ion-stabilized pathway, and the monovalent ion channel as proceeding via a stepwise proton transfer-stabilized pathway.[36] The concerted versus stepwise nature of these pathways was probed by measuring proton inventories in the presence of divalent ions or monovalent ions alone. Proton inventory of 2 in Mg^{2+} and 1 in Na^+ supported the concerted and stepwise nature suggested by the calculations.[33,34] The HDV ribozyme functions in a wide range of monovalent and divalent ions. In the present study, we aimed to broaden our studies to other ions in an effort to determine whether the favored reaction pathway could be dictated by the characteristic of the metal ion in the reaction media. We measured thio effects with a range of monovalent and divalent ions and observed that inverse S_P thio effects occur in the presence of low charge density metal ions, including certain divalent ions. Calculations and experiments were then carried out in an effort to understand the molecular origin of the inverse thio effects associated with low charge density ions, including classical MD trajectories and free energy simulations, QM/MM free energy simulations, rate–pH profiles and proton inventories, and rescue of C75Δ ribozymes with imidazole and NH_4^+.

Possible Origins of the Inverse S_P Thio Effect. Inverse thio effects have been observed previously in phosphorothiolate substitution of the bridging oxygen atom.[24,61] These effects

DOI: 10.1021/acs.biochem.5b00190
Biochemistry 2015, 54, 2160–2175

originate from the higher efficiency of a sulfur atom than an oxygen atom as a leaving group. In the case of nonbridging phosphorothioate substitution, the leaving group remains unaltered. As described in the first part of the Results, an inverse thio effect was observed for the S_P substrate in the presence of low charge density metal ions, and it seems to be a unique finding. Here, we explore the origin of this effect via the two models mentioned in the Results. In Model 1, we consider a possible hydrogen bond between the nucleophilic 2′-OH and *pro*-S_P oxygen on the scissile phosphate. This hydrogen bond would in principle inhibit deprotonation of the 2′-OH and its attack on the phosphorus, and changing the *pro*-S_P oxygen to a sulfur atom might disrupt this hydrogen bond and restore the faster reaction rate (Figure 4, compare panel F to panels D and E). In Model 2, we consider facilitation of the first step of the stepwise mechanism via the presence of sulfur as the *pro*-S_P atom (Figure 6B).

Model 1: Breaking an Inhibitory Hydrogen Bond Between the 2′-OH of U-1 and the Scissile Phosphate. Classical MD trajectories provided evidence for a hydrogen bond between the 2′-OH of U-1 and the scissile phosphate in the presence of Na^+, but not in the presence of an active site Mg^{2+} (Figure S5). In the crystal structure of the precleaved HDV ribozyme, the active site Mg^{2+} coordinates to the 2′O of U-1, as modeled from the hammerhead ribozyme crystal structure PDB ID: 2OEU,[44] and thus may compete for any hydrogen bonding of this hydroxyl group (Figure 4A−C).[37] Hydrogen bonding between the 2′-OH and the scissile phosphate in the presence of Na^+ is indicated by optimal hydrogen bonding angles and distances in one of the two 25 ns classical MD trajectories (Figure S5, green), as well as the free energy simulations focused on U-1 2′-OH interactions (Figure 5). Introduction of a sulfur atom at the *pro*-S_P position is expected to disrupt this hydrogen bond (Figure 4D−F). However, as indicated by one of the classical MD trajectories, while the 2′-OH hydrogen bonds with the *pro*-S_P oxygen part of the time, it hydrogen bonds with the *pro*-R_P oxygen at other times (Figure S5, green). Because of limited sampling in the MD trajectories, we calculated relative free energies between these two states using the more reliable approach combining umbrella sampling and the finite temperature string method. As shown in Figure 5, according to these free energy simulations, the 2′-OH of U-1 donates a hydrogen bond to the *pro*-R_P oxygen in state (6) and to the *pro*-S_P oxygen in state (7), with state (7) favored over state (6) by only 0.5 kcal/mol.

If the 2′-OH of U-1 interacts nearly equally well with either of the nonbridging oxygens of the scissile phosphate, one might expect the R_P and S_P thio effects to be equal and inverse in the presence of Na^+, as opposed to the experimental data showing that the R_P thio effect is normal and the S_P thio effect is inverse. However, we do note that the *pro*-R_P oxygen is also implicated in accepting a proton from the N4 of C75 (Figure 1, lower pathway),[36] a process that might give a big enough normal contribution to the thio effect to offset the inverse contribution. Indeed, observation that the normal R_P thio effect is 1000-fold in 10 mM Mg^{2+} but only 5-fold in 1 M Na^+ is consistent with an inverse contribution to the R_P thio effect in Na^+. Moreover, increase of the normal R_P thio effect to 110-fold and decrease of the inverse S_P thio effect to 2.3-fold upon increasing the Na^+ concentration to 4 M (Figure 2, red) (i.e., both thio effects trending toward 10 mM Mg^{2+} thio effects) also supports this notion: high concentration of Na^+ may lead to occupancy of the Mg^{2+} binding site, which we previously showed has a very negative potential,[46] thus abrogating an intrinsic inverse contribution of sulfur at a nonbridging position and possibly altering the reaction pathway. A similar effect is seen in Li^+ for the R_P substrate (Figure 2A, cyan), also supporting the increasingly normal contribution of the R_P thio effect at high monovalent ion concentrations.

Model 2: Facilitation of a Stepwise Mechanism by Presence of Sulfur at the pro-S_P Position. QM/MM free energy simulations were carried out for the R_P and S_P substrates in Na^+ and Mg^{2+}. In the presence of the active site Mg^{2+} ion, the pathway of each thio substrate was concerted, as previously determined for the oxo substrate, and led to changes in the single free energy barrier that were consistent with previously measured thio effects (Figure 6A). These findings provided validation for pursuing QM/MM free energy simulations in the presence of Na^+.

For the S_P substrate in the presence of Na^+, the pathway was stepwise, as previously determined for the oxo substrate in Na^+, and led to a decrease in the first free energy barrier of 1.5 kcal/mol. As mentioned, the experimental thio effect for the S_P substrate was inverse at 4−7 fold in the presence of group IA monovalent ions at their lower concentrations, consistent with the decrease of the first free energy barrier (Figure 6B).[g]

We previously argued that concordance between the observed experimental rate constant, termed "k_{obs}", and the calculated free energy barriers for the oxo substrate in the presence of Na^+ required inclusion of an 8−10 kcal/mol rapid pre-equilibrium for deprotonation of the 2′-OH, with an equilibrium constant "K_{eq}", prior to cleavage that occurred with a rate constant of "$k_{cleavage}$", or that $k_{obs} = K_{eq}k_{cleavage}$.[36] The MFEP for the S_P substrate in the presence of Na^+ (Figure 6B) is downhill from the thiophosphorane intermediate to the product. Moreover, the barrier from the thiophosphorane intermediate (∼3.5 kcal/mol) to products is small compared to the cumulative barrier preceding the thiophosphorane intermediate (∼10−12 kcal/mol), arguing that this first cumulative barrier is rate-limiting for the S_P substrate. The MFEP for the oxo substrate is similarly downhill,[36] suggesting that it is indeed the comparison of the first barrier that is relevant in the S_P-oxo substrate comparison. As discussed above, for the purposes of analysis by Model 2, we neglect any thio effect on the pre-equilibrium constant, and the free energy barriers of the first step in the cleavage mechanism for the S_P and oxo substrates can be compared directly.

Sulfur, by virtue of its higher polarizability than oxygen, might make the phosphorus more susceptible to nucleophilic attack by the 2′O. Observation that a nonbridging sulfur alters the chemical shift of phosphorus downfield by ∼55 ppm[62] is consistent with deshielding of the phosphorus. In addition, extensive isotope effect and ^{31}P NMR studies on hydrolysis reactions of di- and triester phosphate and their phosphorothioate counterparts have been performed.[63,64] These studies on *p*-nitrophenyl phosphates and phosphorothioates show that the bond order of the phosphorus relative to the leaving group remains unaltered between the phosphate and phosphorothioate esters, indicating no contribution of the scissile ester bond to the enthalpy of reaction.

To conclude, Models 1 and 2 both provide viable explanations for the origin of the inverse S_P thio effect. Model 2, which centers on facilitation of the first step of the stepwise mechanism by virtue of having sulfur at the *pro*-S_P position, can account quantitatively for the observed inverse thio effects in group IA monovalent ions, and dual rescue of

DOI: 10.1021/acs.biochem.5b00190
Biochemistry 2015, 54, 2160−2175

C75Δ by imidazole and NH_4^+ can account for the extra inverse factor for NH_4^+ presented in the Results. However, we caution that statistical error bars on the QM/MM calculations of differences in free energy barriers are ∼1 kcal/mol, and small contributions from Model 1, which centers on breaking of the hydrogen bond between the 2′-OH of U-1 and the *pro*-S_P position, cannot be ruled out. In either of the two models, the inverse thio effect is associated with a stepwise mechanism, either by freeing up the 2′-OH to deprotonate and attack the neighboring phosphorus or by facilitating this attack, possibly through making the phosphorus at the scissile phosphate more susceptible to nucleophilic attack. An inverse S_P thio effect is not observed with Mg^{2+} at the active site, most likely because the phosphorus is already susceptible to attack by the 2′-OH by virtue of its *pro*-R_P oxygen atom being polarized by the chelated Mg^{2+} ion and any 2′-OH-scissile phosphate interaction being broken by the Mg^{2+} ion. Overall, these observations suggest that an inverse thio effect may be diagnostic of a stepwise mechanism for phosphodiester bond cleavage.

Evidence that the Reaction Pathway of the HDV Ribozyme is Controlled by Metal Ion Charge Density. Our current understanding of the main reaction pathways of the HDV ribozyme is depicted in Figure 1. This model is consistent with a wealth of experimental data and theoretical calculations. The upper portion of Figure 1 depicts the reaction pathway in the presence of a high charge density metal ion at the active site such as Mg^{2+}, Ca^{2+}, and Sr^{2+}. Our previous calculations of minimum energy paths (MEPs), which do not include entropic contributions or conformational sampling, indicated that the reaction is concerted with a phosphorane-like transition state when Mg^{2+} or Ca^{2+} is bound at the catalytic site.[31] This mechanism was confirmed using QM/MM free energy simulations, which generated MFEPs and provided free energy barriers that could be used to estimate rate constants.[36]

The reaction free energy barriers from the MFEPs were consistent with experiments on the oxo substrate, as well as on the thio substrates (Figures S7−S10; Table S3).[6,19] Using these reaction free energy barriers (Figures S7−S8 and previous results),[36] we calculated the thio effects from the MFEP of the R_P and S_P substrates in the presence of Mg^{2+} and compared them to experimental results (Table S3). In the presence of Mg^{2+}, the calculated thio effects for the R_P and S_P substrates were 3.03×10^6 and 0.85, respectively (Table S3). The trends agree qualitatively with previous experiments, which indicated a large normal thio effect for the R_P substrate (1000-fold in 10 mM Mg^{2+}) and no thio effect for the S_P substrate (0.97-fold in 10 mM Mg^{2+}).[19] The larger magnitude of the calculated thio effect for the R_P substrate could be due to structural changes as a result of mutating an active site oxygen atom to a bulky sulfur atom, that were not captured by the limited amount of conformational sampling. The free energy barriers determined from the calculations and experiments are also compared in Table S3.

The MFEP calculations also implied that the concerted reaction is more synchronous than suggested by the previously obtained MEP calculations. Earlier proton inventories at low (0.87 mM) and high (10 mM) Mg^{2+} concentrations indicated that two proton transfers occur in the rate-limiting step,[33] presumably deprotonation of the 2′-OH nucleophile and protonation of the 5′O leaving group, consistent with the calculated concerted reaction pathway. Collectively, these results are consistent with occupancy of the upper pathway in Figure 1 in the presence of a high charge density metal ion at the active site, in which the metal ion interacts with the *pro*-R_P oxygen in the transition state. Further support of this metal ion-oxygen interaction came from thiophilic metal ion rescue experiments from our laboratories,[19] as well as observation of "normal" (i.e., noninverted) rate−pH profiles in Mg^{2+} and Ca^{2+},[6] which support a metal-bound hydroxide participating in the reaction.[65] Additionally, as indicated in Table 2, S_P thio effects were either nonexistent (in Mg^{2+}) or very slightly inverse (in Ca^{2+} and Sr^{2+}); this observation is consistent with the 2′-OH being either already freed up and ready to be deprotonated and attack the scissile phosphate (Figure 4A−C) or the phosphorus already being susceptible to attack by the 2′-OH by virtue of polarization of the *pro*-R_P oxygen atom by the site-bound divalent ion.

The lower portion of Figure 1 depicts the reaction pathway in the presence of monovalent and large divalent ions including Li^+, Na^+, K^+, NH_4^+, and Ba^{2+}. The MEP calculations from our laboratories indicated that the reaction is sequential with a phosphorane intermediate in the presence of Li^+, Na^+, and K^+.[31] The MFEP calculations with Na^+ rather than Mg^{2+} at the catalytic site were also consistent with the stepwise mechanism[36] and provided quantitative information on reaction free energy barriers that was consistent with our prior studies on the oxo substrate,[34] as well as on the thio substrates including both normal and inverse thio effects (Tables 1 and S3). In the presence of Na^+, the calculated thio effects for the R_P and S_P substrates were 253 and 1/9.1 (Table S3), respectively. These trends are consistent with the experimental results illustrating thio effects of 39 and 1/7.1 for the R_P and S_P substrates, respectively, in the presence of 2 M Na^+ (Tables 1 and S3).

Prior proton inventories in Na^+ indicated just one proton transfer in the rate-limiting step.[34] Proton inventories in Li^+, NH_4^+, and Ba^{2+} provided herein also indicate just one proton transfer in the rate-limiting step (Figure 7B), consistent with the calculated stepwise reaction pathway. Together, these results support the lower pathway in Figure 1 in the presence of a low charge density metal ion, in which such a metal ion is unable to interact effectively with the nonbridging phosphate oxygens. Instead, a proton transfers from the exocyclic amine of C75 to the *pro*-R_P oxygen to give a phosphorane intermediate. This step is supported experimentally herein by observation that only NH_4^+ ions plus imidazole rescue the ribozyme in the presence of C75Δ in the absence of Mg^{2+} (Table S2), suggesting that the NH_4^+ and imidazole serve as surrogates for the exocyclic N4 and endocyclic N3 atoms, respectively. Observation that NH_4^+ is not needed to rescue C75Δ in the presence of Mg^{2+} for the antigenomic[60] and genomic[6] ribozymes further supports the influence of metal ion charge density on the reaction pathway as illustrated in Figure 1. Additional support of the stepwise reaction pathway comes from inverted rate−pH profiles in Li^+, Na^+, Ba^{2+}, and NH_4^+, which are consistent with an indirect, noncatalytic role of the metal ions in the mechanism.[65] Furthermore, as indicated in Table 1, with the exception of Li^+, S_P thio effects were inverse in these metal ions, which are consistent with either disruption of a 2′-OH−*pro*-S_P hydrogen bond by the sulfur, or the sulfur making the phosphorus more susceptible to attack by the 2′-OH.

In the case of Li^+, the rate−pH profiles are inverted, suggesting a noncatalytic role of Li^+, and the proton inventory is unity suggesting a stepwise mechanism. However, Li^+ has a unique S_P thio effect in that it is normal. All other monovalent

DOI: 10.1021/acs.biochem.5b00190
Biochemistry 2015, 54, 2160−2175

ions and Ba^{2+} had inverse S_P thio effects, while other high charge density divalent ions had no S_P thio effects. One possibility is that because Li^+ is a very hard Lewis acid and S^- is a very soft Lewis base, there is no interaction between them. The absolute hardness of Li^+, Na^+, and K^+ are 35.12, 21.08, and 13.64 eV, respectively.[66,67] The inability of Li^+ to interact with sulfur may raise the free energy of the thiophosphorane intermediate depicted in Figure 1 bottom pathway (and its adjacent transition states) leading to slower rates with the thio substitution.

All of the ions with q/r less than 1.5, which includes NH_4^+, K^+, Na^+, Li^+, and Ba^{2+}, favor a stepwise mechanism in part because these ions appear to not bind in a chelated fashion at the active site, while all of the ions with q/r greater than 1.5, which includes Sr^{2+}, Ca^{2+}, and especially Mg^{2+}, q/r of ∼2.8, favor a metal ion-stabilized concerted mechanism because they bind at the active site (Figure 3). This trend suggests that the weakening Coulombic attractions with the low charge density metal ions provide a major contribution to the inverse thio effect. In addition, the reaction is considerably faster in the high charge density ions, ∼25-fold faster in saturating Mg^{2+} than 1 M Na^+.[16] Related to the above phenomena, another factor driving the concerted mechanism is that the high charge density ions couple anticooperatively with the pK_a of C75, acidifying it[6,28] and driving the proton to the leaving group as the reaction proceeds.[31] In contrast, the low charge density ions do not affect the pK_a of C75,[34] thus not driving proton transfer to the leaving group simultaneously with the 2′-OH attack of the scissile phosphate. Overall, it appears that the charge density of the metal ion in solution plays a significant role in determining the reaction pathway of the HDV ribozyme. It will be of interest to see whether metal ions play similar roles in controlling reaction pathways in other ribozymes.

■ ASSOCIATED CONTENT

Supporting Information

Free energy barriers and standard deviations from statistical error analysis; thio effects in C75Δ ribozyme in monovalent ions only; thio effects in WT ribozyme: comparison of calculated and experimental values; secondary structure of the two-piece ribozyme; QM region of ribozyme; angle coordinates used in free energy simulations; comparison of oxo, R_P, and S_P substrate rates; U-1 2′-OH and nonbridging oxygen distances and angles for oxo, R_P, and S_P substrates; snapshots of the active site at various minima along free energy simulations; QM/MM simulations to obtain the MFEP for the R_P and S_P substrates in the presence of Mg^{2+} or Na^+; proton inventory in 1 M Li^+ as a square-root plot. This material is available free of charge via the Internet at http://pubs.acs.org.

■ AUTHOR INFORMATION

Corresponding Authors

*(S.H.-S.) Telephone: (217) 300-0335; e-mail: shs3@illinois.edu.

*(P.C.B.) Telephone: (814) 863-3812; fax: (814) 865-2927; e-mail: pcb5@psu.edu.

Present Addresses

§(P.T.) Department of Molecular Genomics and Cell Biology University of Chicago, Chicago, IL, 60637.

⊥(A.G.) Max-Planck-Institut für Kohlenforschung, Kaiser-Wilhelm-Platz 1, Mülheim an der Ruhr, 45470, Germany.

Funding

This work was supported by NIH Grant R01GM095923 to P.C.B. and NIH Grant GM056207 to S.H.-S.

Notes

The authors declare no competing financial interest.

■ ACKNOWLEDGMENTS

We thank Andrea Cerrone-Szakal for comments on the manuscript and conversations on proton inventory experiments, and Jamie Bingaman for comments on the manuscript and help with preparing Figure 7. We also thank Tom Mallouk and Tom O'Halloran for helpful discussions.

■ ABBREVIATIONS

HDV, hepatitis delta virus; QM/MM, quantum mechanical/molecular mechanical; R_P/S_P substrate, substrate strand with a sulfur substitution at the nonbridging *pro*-R_P/S_P oxygen on the scissile phosphate; MFEP, minimum free energy path; WT, wild-type

■ ADDITIONAL NOTES

[a]An experiment in 1 M NaCl with renaturation at 90 °C for 2 min, followed by room temperature for 10 min, gave results that were within error of the results from this 55 °C renaturation.

[b]The extent of reactions for the oxo and S_P substrates in the presence of 10 mM Mg^{2+} were ∼85−90%, and the extents of reaction for linearization were assumed to be 100%. The difference in these percentages would underestimate the rate by only 1.1−1.2-fold, which does not significantly affect our results.

[c]Rates in K^+ were sufficiently slow that the rate could only be measured for the S_P substrate and only in K^+ concentrations up to and including 1 M (see Table 1). Previous studies on the two-piece HDV ribozyme also found that the reaction is inhibited in KCl.[6]

[d]The MFEP for the R_P substrate in the presence of Na^+ (Figure S9, Supporting Information) is not downhill. In this case, $k_{cleavage}$ should be taken as the height of the second barrier, or ∼7 kcal/mol. This is 3.5 kcal/mol higher than the first barrier of 3.5 kcal/mol with the oxo substrate.

[e]The reaction was followed up to 3 days with no reaction observed, giving an upper limit of 10^{-6} min^{-1} for any reaction.

[f]These rates may seem low; however, they are not unexpected. Perrotta and Been reported rates for imidazole rescue of the antigenomic ribozyme of 4×10^{-3} min^{-1} in 200 mM imidazole and 10 mM Mg^{2+};[60] extrapolating this rate to 1 M imidazole leads to 20×10^{-3} min^{-1} (no saturation out to 200 mM imidazole was observed). However, the rate of the ribozyme is known to be ∼3000 fold slower in 1 M NaCl than 10 mM Mg^{2+};[16] extrapolating this ionic effect to that estimated above in 1 M imidazole leads to 6.7×10^{-6} min^{-1}, or $\sim 1 \times 10^{-5}$ min^{-1}. Thus, the rates measured herein suggest that ammonium ions can fully participate in the reaction by proton transfer, as described in the text. Note that we chose to extrapolate Perrotta and Been's results on the antigenomic ribozyme since they published the most thorough study including observation of no saturation out to 200 mM imidazole.

[g]We choose the Na^+ concentration range of 0.5−3 M for comparisons, as the similarity of the R_P and S_P thio effects for 4 M Na^+ and 10 mM Mg^{2+} suggests that the pathway may not be sequential at the highest Na^+ concentration.

DOI: 10.1021/acs.biochem.5b00190
Biochemistry 2015, 54, 2160−2175

REFERENCES

(1) Bevilacqua, P. C., and Yajima, R. (2006) Nucleobase catalysis in ribozyme mechanism. *Curr. Opin. Chem. Biol. 10*, 455−464.

(2) Ferré-D'Amaré, A. R., and Scott, W. G. (2010) Small self-cleaving ribozymes. *Cold Spring Harbor Perspect. Biol. 2*, a003574.

(3) Ward, W. L., Plakos, K., and DeRose, V. J. (2014) Nucleic acid catalysis: Metals, nucleobases, and other cofactors. *Chem. Rev. 114*, 4318−4342.

(4) Frederiksen, J. K., and Piccirilli, J. A. (2009) Identification of catalytic metal ion ligands in ribozymes. *Methods 49*, 148−166.

(5) Murray, J. B., Seyhan, A. A., Walter, N. G., Burke, J. M., and Scott, W. G. (1998) The hammerhead, hairpin and VS ribozymes are catalytically proficient in monovalent cations alone. *Chem. Biol. 5*, 587−595.

(6) Nakano, S., Chadalavada, D. M., and Bevilacqua, P. C. (2000) General acid-base catalysis in the mechanism of a hepatitis delta virus ribozyme. *Science 287*, 1493−1497.

(7) Perrotta, A. T., and Been, M. D. (2006) HDV ribozyme activity in monovalent cations. *Biochemistry 45*, 11357−11365.

(8) Roth, A., Nahvi, A. L. I., Lee, M., Jona, I., and Breaker, R. R. (2006) Characteristics of the glmS ribozyme suggest only structural roles for divalent metal ions. *RNA 12*, 607−619.

(9) Roth, A., Weinberg, Z., Chen, A. G. Y., Kim, P. B., Ames, T. D., and Breaker, R. R. (2014) A widespread self-cleaving ribozyme class is revealed by bioinformatics. *Nat. Chem. Biol. 10*, 56−60.

(10) Nesbitt, S., Hegg, L. A., and Fedor, M. J. (1997) An unusual pH-independent and metal-ion-independent mechanism for hairpin ribozyme catalysis. *Chem. Biol. 4*, 619−630.

(11) Hampel, A., and Cowan, J. A. (1997) A unique mechanism for RNA catalysis: the role of metal cofactors in hairpin ribozyme cleavage. *Chem. Biol. 4*, 513−517.

(12) Basolo, R., and Pearson, R. G. (1988) *Mechanisms of Inorganic Reactions*, 2nd ed., pp 164−165, John Wiley & Sons Inc., New York.

(13) Gong, B., Chen, J.-H., Bevilacqua, P. C., Golden, B. L., and Carey, P. R. (2009) Competition between $Co[(NH_3)_6]^{3+}$ and inner sphere Mg^{2+} ions in the HDV ribozyme. *Biochemistry 48*, 11961−11970.

(14) Roychowdhury-Saha, M., and Burke, D. H. (2007) Distinct reaction pathway promoted by non-divalent-metal cations in a tertiary stabilized hammerhead ribozyme. *RNA 13*, 841−848.

(15) Horton, T. E., and DeRose, V. J. (2000) Cobalt hexammine inhibition of the hammerhead ribozyme. *Biochemistry 39*, 11408−11416.

(16) Nakano, S., Proctor, D. J., and Bevilacqua, P. C. (2001) Mechanistic characterization of the HDV genomic ribozyme: assessing the catalytic and structural contributions of divalent metal ions within a multichannel reaction mechanism. *Biochemistry 40*, 12022−12038.

(17) Curtis, E. A., and Bartel, D. P. (2001) The hammerhead cleavage reaction in monovalent cations. *RNA 7*, 546−552.

(18) O'Rear, J. L., Wang, S., Feig, A. L., Beigelman, L., Uhlenbeck, O. C., and Herschlag, D. (2001) Comparison of the hammerhead cleavage reactions stimulated by monovalent and divalent cations. *RNA 7*, 537−545.

(19) Thaplyal, P., Ganguly, A., Golden, B. L., Hammes-Schiffer, S., and Bevilacqua, P. C. (2013) Thio effects and an unconventional metal ion rescue in the genomic hepatitis delta virus ribozyme. *Biochemistry 52*, 6499−6514.

(20) Salehi-Ashtiani, K., Lupták, A., Litovchick, A., and Szostak, J. W. (2006) A genomewide search for ribozymes reveals an HDV-like sequence in the human CPEB3 gene. *Science 313*, 1788−1792.

(21) Webb, C.-H. T., Riccitelli, N. J., Ruminski, D. J., and Lupták, A. (2009) Widespread occurrence of self-cleaving ribozymes. *Science 326*, 953.

(22) Riccitelli, N., and Lupták, A. (2013) HDV family of self-cleaving ribozymes. *Prog. Mol. Biol. Transl. Sci.*, 123−171.

(23) Golden, B. L., Hammes-Schiffer, S., Carey, P. R., and Bevilacqua, P. C. (2013) An integrated picture of HDV ribozyme catalysis, in *Biophysics of RNA Folding* (Russell, R., Ed.) pp 135−168. Springer, New York.

(24) Das, S. R., and Piccirilli, J. A. (2005) General acid catalysis by the hepatitis delta virus ribozyme. *Nat. Chem. Biol. 1*, 45−52.

(25) Lee, T. S., Giambaşu, G. M., Harris, M. E., and York, D. M. (2011) Characterization of the structure and dynamics of the hdv ribozyme in different stages along the reaction path. *J. Phys. Chem. Lett. 2*, 2538−2543.

(26) Kapral, G. J., Jain, S., Noeske, J., Doudna, J. A., Richardson, D. C., and Richardson, J. S. (2014) New tools provide a second look at HDV ribozyme structure, dynamics and cleavage. *Nucleic Acids Res. 42*, 12833−12846.

(27) Sripathi, K. N., Tay, W. W., Banas, P., Otyepka, M., Sponer, J., and Walter, N. G. (2014) Disparate HDV ribozyme crystal structures represent intermediates on a rugged free-energy landscape. *RNA 20*, 1112−1118.

(28) Gong, B., Chen, J.-H., Chase, E., Chadalavada, D. M., Yajima, R., Golden, B. L., Bevilacqua, P. C., and Carey, P. R. (2007) Direct measurement of a pK(a) near neutrality for the catalytic cytosine in the genomic HDV ribozyme using Raman crystallography. *J. Am. Chem. Soc. 129*, 13335−13342.

(29) Guo, M., Spitale, R. C., Volpini, R., Krucinska, J., Cristalli, G., Carey, P. R., and Wedekind, J. E. (2009) Direct Raman measurement of an elevated base pKa in the active site of a small ribozyme in a precatalytic conformation. *J. Am. Chem. Soc. 131*, 12908−12909.

(30) Gong, B., Klein, D. J., Ferré-D'Amaré, A. R., and Carey, P. R. (2011) The glmS ribozyme tunes the catalytically critical pK(a) of its coenzyme glucosamine-6-phosphate. *J. Am. Chem. Soc. 133*, 14188−14191.

(31) Ganguly, A., Bevilacqua, P. C., and Hammes-Schiffer, S. (2011) Quantum mechanical/molecular mechanical study of the HDV ribozyme: impact of the catalytic metal ion on the mechanism. *J. Phys. Chem. Lett. 2*, 2906−2911.

(32) Heldenbrand, H., Janowski, P. A., Giambaşu, G., Giese, T. J., Wedekind, J. E., and York, D. M. (2014) Evidence for the role of active site residues in the hairpin ribozyme from molecular simulations along the reaction path. *J. Am. Chem. Soc. 136*, 7789−7792.

(33) Nakano, S., and Bevilacqua, P. C. (2001) Proton inventory of the genomic HDV ribozyme in Mg^{2+}-containing solutions. *J. Am. Chem. Soc. 123*, 11333−11334.

(34) Cerrone-Szakal, A. L., Siegfried, N. A., and Bevilacqua, P. C. (2008) Mechanistic characterization of the HDV genomic ribozyme: solvent isotope effects and proton inventories in the absence of divalent metal ions support C75 as the general acid. *J. Am. Chem. Soc. 130*, 14504−14520.

(35) Chen, J., Ganguly, A., Miswan, Z., Hammes-Schiffer, S., Bevilacqua, P. C., and Golden, B. L. (2013) Identification of the catalytic Mg^{2+} ion in the hepatitis delta virus ribozyme. *Biochemistry 52*, 557−567.

(36) Ganguly, A., Thaplyal, P., Rosta, E., Bevilacqua, P. C., and Hammes-Schiffer, S. (2014) Quantum mechanical/molecular mechanical free energy simulations of the self-cleavage reaction in the hepatitis delta virus ribozyme. *J. Am. Chem. Soc. 136*, 1483−1496.

(37) Chen, J.-H., Yajima, R., Chadalavada, D. M., Chase, E., Bevilacqua, P. C., and Golden, B. L. (2010) A 1.9 Å crystal structure of the HDV ribozyme precleavage suggests both Lewis acid and general acid mechanisms contribute to phosphodiester cleavage. *Biochemistry 49*, 6508−6518.

(38) Chadalavada, D. M., Cerrone-Szakal, A. L., Wilcox, J. L., Siegfried, N. A., and Bevilacqua, P. C. (2012) Mechanistic analysis of the hepatitis delta virus ribozyme. *Methods Mol. Biol. 848*, 21−40.

(39) Schowen, B. K., and Schowen, R. L. (1982) Solvent isotope effects on enzyme systems. *Methods Enzymol. 87*, 551−606.

(40) Anslyn, E., and Breslow, R. (1989) Proton inventory of a bifunctional ribonuclease model. *J. Am. Chem. Soc. 111*, 8931−8932.

(41) *Desmond Molecular Dynamics System*, v. 2.2 (2009) D. E. Shaw Research, New York.

(42) Cornell, W. D., Cieplak, P., Bayly, C. I., Gould, I. R., Merz, K. M., Ferguson, D. M., Spellmeyer, D. C., Fox, T., Caldwell, J. W., and Kollman, P. A. (1995) A second generation force field for the

DOI: 10.1021/acs.biochem.5b00190
Biochemistry 2015, 54, 2160−2175

simulation of proteins, nucleic acids, and organic molecules. *J. Am. Chem. Soc. 117*, 5179−5197.
(43) Veeraraghavan, N., Ganguly, A., Golden, B. L., Bevilacqua, P. C., and Hammes-Schiffer, S. (2011) Mechanistic strategies in the HDV ribozyme: chelated and diffuse metal ion interactions and active site protonation. *J. Phys. Chem. B 115*, 8346−8357.
(44) Martick, M., and Scott, W. G. (2006) Tertiary contacts distant from the active site prime a ribozyme for catalysis. *Cell 126*, 309−320.
(45) Veeraraghavan, N., Bevilacqua, P. C., and Hammes-Schiffer, S. (2010) Long-distance communication in the HDV ribozyme: insights from molecular dynamics and experiments. *J. Mol. Biol. 402*, 278−291.
(46) Veeraraghavan, N., Ganguly, A., Chen, J.-H., Bevilacqua, P. C., Hammes-Schiffer, S., and Golden, B. L. (2011) Metal binding motif in the active site of the HDV ribozyme binds divalent and monovalent ions. *Biochemistry 50*, 2672−2682.
(47) Nakano, S., and Bevilacqua, P. C. (2007) Mechanistic characterization of the HDV genomic ribozyme: a mutant of the C41 motif provides insight into the positioning and thermodynamic linkage of metal ions and protons. *Biochemistry 46*, 3001−3012.
(48) Shao, Y., Molnar, F., Jung, Y., Brown, S. T., Gilbert, A. T. B., Slipchenko, L. V., Levchenko, S. V., Neill, D. P. O., Jr, A. D., Rohini, C., Wang, T., Beran, G. J. O., Besley, N. A., John, M., Lin, Y., Voorhis, T. Van, Chien, H., Sodt, A., Steele, P., Rassolov, V. A., Maslen, P. E., Korambath, P. P., Adamson, D., Austin, B., Baker, J., Byrd, E. F. C., Dachsel, H., Doerksen, R. J., Dreuw, A., Dunietz, B. D., Dutoi, A. D., Furlani, T. R., Gwaltney, S. R., Heyden, A., Hirata, S., Hsu, P., Kedziora, G., Khalliulin, R. Z., Klunzinger, P., Aaron, M., Lee, M. S., Liang, W., Lotan, I., Nair, N., Peters, B., Proynov, E. I., Pieniazek, P. A., Rhee, M., Ritchie, J., Sherrill, C. D., Simmonett, A. C., Subotnik, J. E., Lee, H., Iii, W., Zhang, W., Bell, A. T., Chakraborty, A. K., Daniel, M., Keil, F. J., Warshel, A., Hehre, W. J., Schaefer, H. F., Kong, J., Krylov, A. I., Gill, M. W., and Head-Gordon, M. (2006) Advances in methods and algorithms in a modern quantum chemistry program package. *Phys. Chem. Chem. Phys. 8*, 3172−3191.
(49) Brooks, B. R., Bruccoleri, R. E., Olafson, B. D., States, D. J., Swaminathan, S., and Karplus, M. (1983) CHARMM: A program for macromolecular energy, minimization, and dynamics calculations. *J. Comput. Chem. 4*, 187−217.
(50) Becke, A. D. (1993) A new mixing of Hartree−Fock and local density-functional theories. *J. Chem. Phys. 98*, 1372−1377.
(51) Rosta, E., Nowotny, M., Yang, W., and Hummer, G. (2011) Catalytic mechanism of RNA backbone cleavage by ribonuclease H from quantum mechanics/molecular mechanics simulations. *J. Am. Chem. Soc. 133*, 8934−8941.
(52) Zhang, S., Ganguly, A., Goyal, P., Bingaman, J., Bevilacqua, P. C., and Hammes-Schiffer, S. (2015) Role of the active site guanine in the glms ribozyme self-cleavage mechanism: Quantum mechanical/molecular mechanical free energy simulations. *J. Am. Chem. Soc. 137*, 784−798.
(53) Izatt, R. M., Christensen, J. J., and Rytting, J. H. (1971) Sites and thermodynamic quantitities associated with proton and metal ion interaction with ribonucleic acid, deoxyribonucleic acid, and their constituent bases, nucleosides, and nucleotides. *Chem. Rev. 71*, 439−481.
(54) Juneau, K., Podell, E., Harrington, D. J., and Cech, T. R. (2001) Structural basis of the enhanced stability of a mutant ribozyme domain and a detailed view of RNA-solvent interactions. *Structure 9*, 221−231.
(55) Cate, J. H., Hanna, R. L., and Doudna, J. A. (1997) A magnesium ion core at the heart of a ribozyme domain. *Nat. Struct. Biol. 4*, 553−558.
(56) Nakano, S., Cerrone, A. L., and Bevilacqua, P. C. (2003) Mechanistic characterization of the HDV genomic ribozyme: classifying the catalytic and structural metal ion sites within a multichannel reaction mechanism. *Biochemistry 42*, 2982−2994.
(57) Wrzesinski, J., Wichłacz, A., Nijakowska, D., Rebowska, B., Nawrot, B., and Ciesiołka, J. (2010) Phosphate residues of antigenomic HDV ribozyme important for catalysis that are revealed by phosphorothioate modification. *New J. Chem. 34*, 1018−1026.
(58) Rosenstein, S. P., and Been, M. D. (1991) Evidence that genomic and antigenomic RNA self-cleaving elements from hepatitis delta virus have similar secondary structures. *Nucleic Acids Res. 19*, 5409−5416.
(59) Lévesque, D., Reymond, C., and Perreault, J. P. (2012) Characterization of the trans Watson-Crick GU base pair located in the catalytic core of the antigenomic HDV ribozyme. *PLoS One 7*, e40309.
(60) Perrotta, A. T., Shih, I., and Been, M. D. (1999) Imidazole rescue of a cytosine mutation in a self-cleaving ribozyme. *Science 286*, 123−126.
(61) Zhao, L., Liu, Y., Bruzik, K. S., and Tsai, M. D. (2003) A novel calcium-dependent bacterial phosphatidylinositol-specific phospholipase C displaying unprecedented magnitudes of thio effect, inverse thio effect, and stereoselectivity. *J. Am. Chem. Soc. 125*, 22−23.
(62) Moody, E. M., Brown, T. S., and Bevilacqua, P. C. (2004) Simple method for determining nucleobase pKa values by indirect labeling and demonstration of a pKa of neutrality in dsDNA. *J. Am. Chem. Soc. 126*, 10200−10201.
(63) Catrina, I. E., and Hengge, A. C. (2003) Comparisons of phosphorothioate with phosphate transfer reactions for a monoester, diester, and triester: isotope effect studies. *J. Am. Chem. Soc. 125*, 7546−7552.
(64) Purcell, J., and Hengge, A. C. (2005) The thermodynamics of phosphate versus phosphorothioate ester hydrolysis. *J. Org. Chem. 70*, 8437−8442.
(65) Bevilacqua, P. C. (2003) Mechanistic considerations for general acid-base catalysis by RNA: revisiting the mechanism of the hairpin ribozyme. *Biochemistry 42*, 2259−2265.
(66) Feig, A. L., and Uhlenbeck, O. C. (1999) The RNA World, 2nd ed., pp 290−291, Cold Spring Harbor Laboratory Press, Cold Spring Harbor, NY.
(67) Pearson, R. G. (1988) Absolute electronegativity and hardness: application to inorganic chemistry. *Inorg. Chem. 27*, 734−740.
(68) Bevington, P. R. (1969) *Data Reduction and Error Analysis for the Physical Sciences*, pp 56−65, McGraw-Hill, New York.
(69) Richens, D. (1997) *The Chemistry of Aqua Ions: Synthesis, Structure and Reactivity*, pp 577−582, John Wiley & Sons Inc., New York.
(70) Masterton, W. L., Bolocofsky, D., and Lee, T. P. (1971) Ionic Radii from scaled particle theory of the salt effect. *J. Phys. Chem. 76*, 2809−2815.

DOI: 10.1021/acs.biochem.5b00190
Biochemistry 2015, 54, 2160−2175